Material Science and Technology Division

Propulsion Materials Program
Quarterly Progress Report for
October through December 2010

D. R. Johnson
Technical Project Manager

Prepared for
U.S. Department of Energy
Assistant Secretary for Energy Efficiency and Renewable Energy
Office of Vehicle Technologies Program
VT 05 04 000

Prepared by the
OAK RIDGE NATIONAL LABORATORY
Oak Ridge, Tennessee 37831-6066
Managed by
UT-Battelle, LLC
for the Department of Energy
Under contract DE-AC05-00OR22725

CONTENTS

Project 18516 – Materials for Hybrid and Electric Drive Systems

Agreement 23279 - Improved Organics for Power Electronics and Electric Motors *(ORNL)*

Agreement 23278 - Low-Cost Direct Bonded Aluminum (DBA) Substrates *(ORNL)*

Agreement 19201 – MBD Non-Rare Earth Magnetic Materials *(ORNL)*

Project 18518 – Materials for High Efficiency Engines

Agreement 11752 – Materials for HCCI Engines *(ORNL)*

Agreement 13329 – Mechanical Reliability of PS Actuators *(ORNL)*

Agreement 15050 – Evaluation of Materials via ACERT Engine *(ORNL)*

Agreement 16303 – Materials for High Pressure Fuel Injection Systems *(ORNL)*

Agreement 16304 – Materials for Advanced Engine Valve Train *(ORNL)*

Agreement 17257 – Materials for Advanced Turbocharger Design *(ORNL)*

Agreement 17894 – NDE for ACERT Engine Components *(ANL)*

Agreement 18570 – Engine Materials Compatibility with Alternate Fuels *(ORNL)*

Agreement 18571 – Materials Issues Associated with EGR Systems *(ORNL)*

Agreement 19202 – Titanium Friction and Wear *(ORNL)*

Project 18519 – Materials for Exhaust and Energy Recovery

Agreement 10635 – Catalysts via First Principles *(ORNL)*

Agreement 19214 - Biofuels Impact on Diesel Particulate Filters *(ORNL)*

Agreement 20091 – Electrically Regenerated DPF Material *(ORNL)*

<u>Project 18865 – Materials by Design</u>

Agreement 9105 – Characterization of Catalyst Microstructures *(ORNL)*

Agreement 14957 – Thermoelectric Mechanical Reliability *(ORNL)*

Agreement 16308 – MBD - Thermoelectrics Theory and Structure *(ORNL)*

Agreement 23279: Improved Organics for Power Electronics and Electric Motors

A. A. Wereszczak, C. W. Ayers, and H. -T. Lin
Oak Ridge National Laboratory

Objective/Scope

Identify lower-cost and better-performing organic compounds for dielectric and thermal management applications in power electronics and electric motors. Candidate and new organic compounds (e.g., epoxy molded compounds or EMCs) will be characterized and developed to promote low-cost fabrication, volume reduction, mechanically resilience, and improved and alternative thermal management exploitation. They include compounds presently used in dielectrics in power electronic devices, potting compounds used with capacitors, and pottings used in motors. For dielectrics, improved performance represents a higher-temperature capability and the sustainment of dielectric and gel-like mechanical damping properties under thermal cycling and vibratory conditions. For potting compounds used with capacitors or motors, interest exists to identify alternatives that have higher thermal conductivity (or that enhance the thermal conductivity of existing compounds) or that benefit structural or damping performance without compromising thermal performance.

Technical Highlights

None yet because this new project has not yet received financial support. However, a concept for a high thermally conductive and electrically insulative is under development and the submittal of an invention disclosure for it is anticipated in FY11Q2.

Status of FY 2010 Milestones

1. Establish baselines by measuring thermal properties of unused and serviced organics of each of three classes of organics. [Jun11] *May be difficult to satisfy by Jun11 due to ongoing CR.*
2. Develop test methods that representatively thermal cycle each of the three classes of organic materials. [Sep11] *On schedule.*

Communications/Visits/Travel

Several technical discussions have occurred with NTRC's C. Ayers.

Problems Encountered

Project not officially started because funding support has not been provided yet.

Publications/Presentations/Awards

None.

References

None.

Agreement 23278: Low-Cost Direct Bonded Aluminum (DBA) Substrates

H. -T. Lin and A. A. Wereszczak
Oak Ridge National Laboratory

Objective/Scope

This project seeks to develop low-cost, high quality, and thermomechanically robust direct-bonded aluminum (DBA) substrates. Low-cost DBA substrates will lessen the cost of the inverter insulated gate bipolar transistor (IGBT) power modules while concomitantly sustaining or improving thermal management and improving thermomechanical reliability. Compared to copper and DBC substrates, aluminum has a lower elastic modulus so it imparts a lower stress on the ceramic substrate it sandwiches, and this contributes to improved mechanical reliability of the entire substrate. Wire and ribbon for bonding in power electronic modules tends to be aluminum, so the apparent coefficient of thermal expansion of DBAs is compatible with them unlike DBCs. The use of a DBA substrate will also lessen the weight up to 50% compared to presently used DBC substrates, and this would contribute to the weight reduction goals of the inverter and converter in the APEEM program as well.

Technical Highlights

None yet because this new project has not yet received financial support. However, a concept for a high thermally conductive and electrically insulative is under development and the submittal of an invention disclosure for it is anticipated in FY11Q2.

Status of FY 2010 Milestones

1. Survey conventional and alternative processing methods to directly bond Al to Al_2O_3 (and AlN). [Apr11] *Unlikely to satisfy by Apr11 due to ongoing CR.*
2. Down-select processing method most likely to produce high strength bonding. [Sep11] *Uncertainty exists about satisfying this by Sep11 due to ongoing CR.*

Communications/Visits/Travel

Several discussions have occurred with ONRL/NTRC and General Motors staffs about the plans for this project.

Problems Encountered

Project not officially started because funding support has not been provided yet.

Publications/Presentations/Awards

None.

References

None.

Agreement 19201: Non-Rare Earth Magnetic Materials

Michael A. McGuire and David J. Singh
Oak Ridge National Laboratory

Nirmal Ghimire
University of Tennessee

Objective/Scope

We will examine rare-earth-free chemical systems which hold promise for the discovery of new high-temperature ferromagnets with the large magnetic moments and strong anisotropies required for technologically useful permanent magnet materials. This research will focus on the development of new rare-earth free permanent magnet materials. Understudied chemical systems which are likely to contain materials with properties required for useful ferromagnets (large moments, high Curie temperatures, strong magnetic anisotropy) will be synthesized and characterized. First principle calculations will be performed to aid in the identification of promising target materials and to guide chemical tuning of magnetic properties through element substitutions and alloying. The focus will be on materials based on elements, such as Mn, Fe and Cr, suitable for application in vehicles.

The primary challenge in this work is to obtain high magnetic anisotropy without rare-earth elements, while maintaining high saturation magnetization. The two main sources of anisotropy are magneto-crystalline anisotropy and shape anisotropy. Magneto-crystalline anisotropy is an intrinsic property determined by energy required to rotate a magnetic moment relative to the crystal lattice. Shape anisotropy is an extrinsic property related to the domain structure of individual crystallites. We are targeting intermetallic compounds with large magneto-crystalline anisotropy, which could then be further enhanced by materials processing to optimize magnetic domain configurations. To obtain anisotropic magnetic properties, heavy transition metal elements will be incorporated instead of rare earths.

Technical Highlights

Hf_2Co_{11} was identified as a promising material during our investigations in FY2010. In this quarter, we have continued our study of our melt-spun samples. In particular, the effects of annealing have been investigated. Below we show the effects of short heat treatments (2 day at temperature, in vacuum) on the x-ray diffraction pattern (Figure 1), the saturation magnetization (Figure 2), and the demagnetization curve (Figure 3).

Although the gross structure of the diffraction patterns shown in Figure 1 remains the same, a systematic evolution is observed as the annealing temperature is varied. A detailed analysis of the changes must await a better understanding of the crystal structures of Hf_2Co_{11} and related compounds. However, these results confirm that the main phase(s) present in the melt-spun material is robust against exposure to elevated temperatures, at least for a short time. The appearance of well defined peaks at high

angle in the 600 and 800 C annealed samples suggest that the crystallinity is improved by heating to these temperatures.

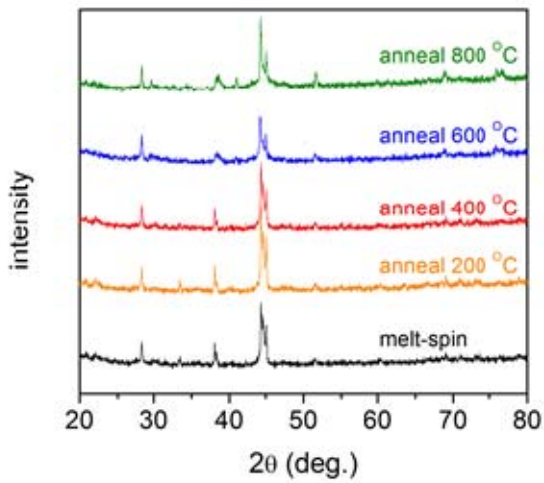

Figure 1. Room temperature Cu Kα powder x-ray diffraction patterns from the surface of melt-spun and annealed ribbons of Hf_2Co_{11}.

The magnetization curves shown in Figure 2 reveal that the saturation moment is decreased systematically by annealing. For the highest annealing temperature, the moment is nearly saturated at 60 kOe. In addition, the moment approaches saturation more rapidly in this sample, suggesting softer magnetic behavior.

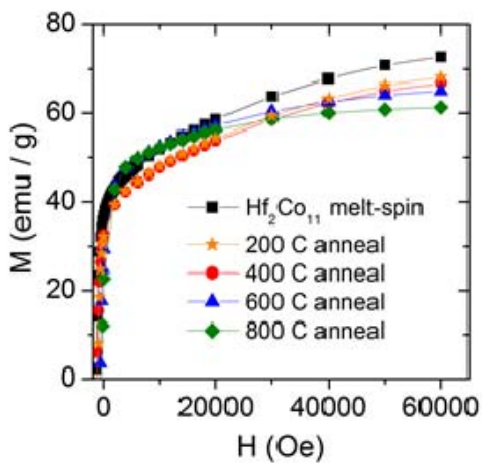

Figure 2. Magnetization vs. applied field for melt-spun and annealed ribbons of Hf_2Co_{11}, showing the effects of heat treatment on the saturation moment.

A softening of the magnetic behavior induced by annealing is also seen in the demagnetization curves in Figure 3. Heat treatment degrades the remanence and the coercivity, and the material becomes quite soft after the highest temperature anneals.

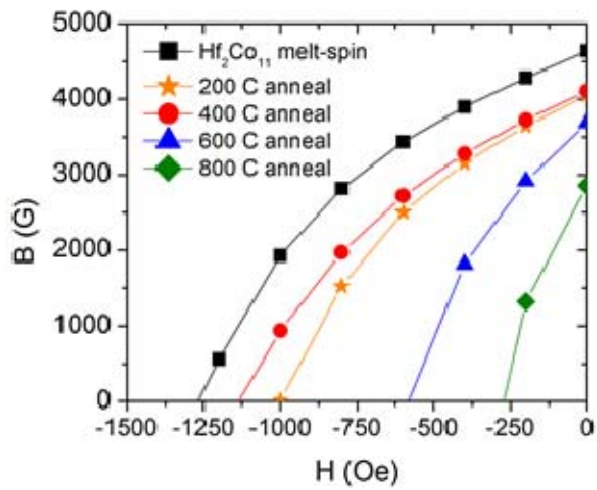

Figure 3. Demagnetization curves for melt-spun and annealed ribbons of Hf_2Co_{11}, showing magnetic softening due to heat treatment.

Effects of annealing on the Curie temperature and microstructure are planned for later in FY2011.

Other work in this quarter included ongoing study of other intermetallics in systems based on μ-phases and Laves phases. Preliminary experiments and literature reviews on the effects of nitrogen in hard magnets indicates the synthetic challenges and stability issues likely may limit the utility of these materials. Other light elements are being considered.

Status of FY 2011 Milestones

We have continued our study of the Hf-Co system by studying annealing effects on samples with composition Hf_2Co_{11}.

Communications/Visits/Travel

The FY2011 Kickoff Meeting for the Vehicles Technologies Program Advanced Power Electronics and Electric Motors R&D (APEEM) was attended at the conference center at ORNL. The meeting involved presentations and discussions with industry representatives and other magnet researchers.

Problems Encountered

Magnetic characterization of materials became a bottleneck during this quarter. The magnetometer, shared by this and several BES programs, was heavily used. Options for magnetic measurements in other existing, similar measurement systems are being explored.

Publications/Presentations/Awards

Poster Presentation: APEEM FY2011 Kickoff Meeting, ORNL.

References

None

Agreement 11752: Advanced Materials Development through Computational Design for HCCI Engine Applications

Govindarajan Muralidharan, Rick Battiste, and Bruce G. Bunting
Oak Ridge National Laboratory

Objectives/Scope

To identify and catalog the materials operating conditions in the HCCI engines and utilize computational design concepts to develop advanced materials for such applications.

Highlights

Technical Progress

Materials-by-Design of Advanced Materials:

In this quarter, work was continued on Ni-based alloys for valve applications. As reported earlier, using thermodynamic modeling, microstructure evaluation, and mechanical property evaluation, high temperature fatigue was identified as a property of critical interest in Ni-based alloy valve materials for the next generation automotive engines. In order to develop relationships between the microstructures of the alloys and their mechanical properties, high-temperature fatigue property data were obtained on all down-selected alloys as a part of the project. Using the approximate correlation between the fatigue lives obtained using the rotating beam and fully reversed fatigue testing techniques several alloys with required microstructures have been identified as candidates for high temperature valve applications.

Using the microstructures of these alloys as a guide, computational thermodynamics was used to identify additional alloys with microstructure similar to the commercial alloys with desirable properties. In contrast to the commercially available alloys with Ni-contents in the range of 50 wt % to 60 wt %, the Ni-content in these alloys ranges from about 30 wt % to 45 wt % with the potential to achieve comparable properties. This implies that the alloys will be of lower cost but comparable mechanical properties.

In this quarter two alloys (HCCI-9, HCCI-16) (see Figure 1) have been down-selected and prepared in the form of large plates. Three additional alloys (HCCI-20, HCCI-34, HCCI-35) have been prepared in smaller batches and have been rolled (see Figure 2). Both tensile specimens and fatigue specimens have been prepared from these alloys and room temperature and high temperatures tensile tests have been completed on these alloys. Table 1 shows a summary of the yield strengths of the alloys at 870°C. ***Note that the yield strengths of all the alloys at the temperature of interest are greater than 35Ksi, the stress level of interest in the valve application, which is a significant achievement in the project***. In addition, these alloys have been aged at 870°C for 216 hours to simulate the effect of long-term exposure at high temperatures on the yields strengths of these alloys. Figure 3 shows a summary of the loss of yield strength of these alloys during this aging condition. Note that certain alloys show larger

loss of strength than other alloys. Fatigue tests are currently underway to compare the high temperature fatigue properties of these alloys.

Table 1

Alloy	**Yield Strength at 870°C (Ksi)**
HCCI-9	63.4
HCCI-16	71.5
HCCI-20	54.5
HCCI-34	61.2
HCCI-35	60.5

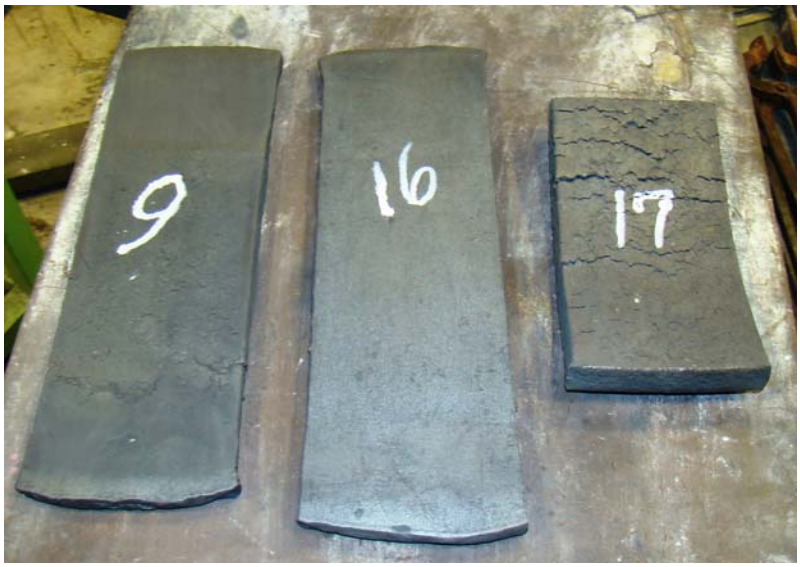

Figure 1. Two Large Heats of Alloys Were Cast (HCCI-9, HCCI-16) and Successfully Fabricated into Plates for Specimen Machining

Figure 2. Three Additional Smaller Heats of Alloys (HCCI-20, HCCI-34, HCCI-35) Were Cast and Successfully Fabricated into Plates for Specimen Machining

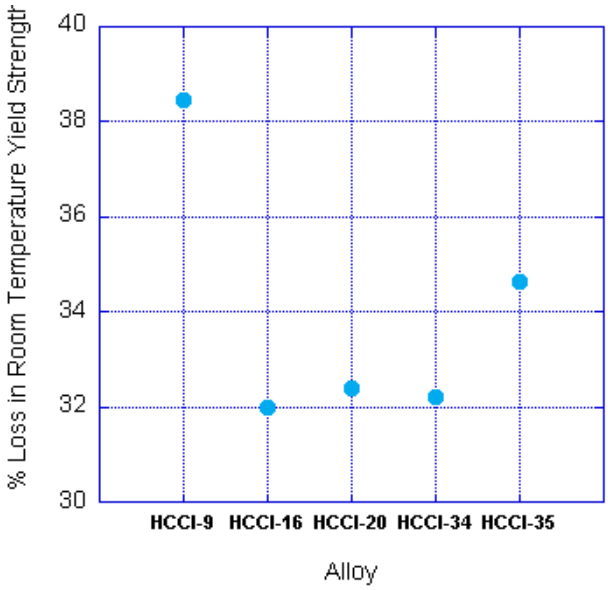

Figure 3. Effect of High Temperature Aging on the High Temperature Yield Strength of ORNL-Developed Alloys

Milestones

Work is on target to meet the following milestones:

- Present progress detailing results on the high temperature tensile testing and fatigue testing of new ORNL-developed alloys at the Annual Merit Review
- Identify a path for the further development of exhaust valve alloys (7/2011)

Agreement 13329: Design Optimization of Piezoceramic Multilayer Actuators for Heavy Duty Diesel Engine Fuel Injectors

H.-T. Lin, H. Wang, T. Matsunaga, and A. A. Wereszczak
Oak Ridge National Laboratory

R. Stafford and D. Memering
Cummins Inc.

Objective/Scope

Enable confident utilization of piezo stack actuator in fuel injectors for heavy vehicle diesel engines. The use of such actuators in diesel fuel injectors has the potential to reduce injector response time, provide greater precision and control of the fuel injection event, and lessen energy consumption. Though piezoelectric function is the obvious primary function of lead zirconate titanate (PZT) ceramic stacks for fuel injectors, their mechanical reliability can be a performance and life limiter because PZT is brittle, lacks high strength, and is susceptible to fatigue. However, that brittleness, relatively low strength, and fatigue susceptibility can be overcome with the use of appropriate probabilistic design methods.

Technical Highlights

1. Mechanical Test and Characterization in High Electric Field

Proposed testing in this stage is a part of ball-on-ring studies on KCI (Kinetic Ceramics, Inc.) PZT, especially, the electric field effect on the flexure strength. Previous tests showed that a certain effect of electric field existed when the field range was within $\pm E_c$ (coercive field). Now it is suggested to investigate the trend if the electric field goes beyond this range. Previous tests also showed that dielectric breakdown occurred near the contact when the electric field increased to $2E_c$. An oil bath system has thus been designed and fabricated to include an electronic fluid (FC-40) as a working environment so as to control the partial charge due to the dielectric breakdown. These KCI plates were supplied by Cummins, Inc. earlier time of FY2010. The coercive field of KCI PZT material is 1.05 kV/mm. Some of them were used in the electric cyclic fatigue study using piezodilatometer. The fatigue response of this PZT material has been observed to be quite typical of soft PZT. Ball-on-ring tests were conducted in an in-house indentation system. The setup of test specimen and mechanical loading are precisely controlled using XYZ motors. A video camera system is also used so that the alignment and loading can be monitored.

The electric loading was obtained through a high voltage amplifier (Trek 609E-6). The applied voltage was defined according to the designed electric field and thickness of specimen. Positive and negative electric fields were applied by setting the positive and

negative electrodes into tension, respectively. For all of the supplied specimens, the positive sides had been marked by the manufacturer. Input waveform was generated and supplied by a LABVIEW program.

1) A trapezoidal waveform was used: a rising time less than 10 seconds, holding time 10 seconds and allowing time more than 60 seconds for mechanical loading, and falling time another 10 seconds.
2) The maximum voltage in function generator was defined: the target volt in a specified loading case can be obtained after amplified 1000 (gain of amplifier).

To measure and monitor the applied electric field during the test, the outputs of voltage and electric current were connected into DAQ system.

The oil bath system is mounted onto the stage (HPS-170, miCos, Eschbach, Germany) of indentation system, as shown in Fig. 1a. The bottom of joint plate is sealed to the base plate of oil bath by using epoxy, and so are all the corners and connection points. The sealing tape is used in bolts on the top surface of joint plate. The support ring is a metal disk with center hole whose diameter is 9.5 mm. It is equipped with a horizontal hole aside accommodating the high voltage wire. The metal ball is of 6.35mm diameter and bearing grade. The ball is attached to the lower end of spindle by using a conductive resin (TIGA Silver 901, Resin Easton, MA) and the spindle itself is grounded and connected to the HV amplifier.

With all of the components assembled, the ball-on-ring setup was aligned to the loading spindle by using XY motors via the LABVIEW program. The elevation of loading ball was adjusted as it is necessary. Lowering the spindle creates a Hertzian contact with the surface of specimen. As the specimens were coated with aluminum on both sides, this creates an electric contact as well. A force of ~2 N was used for initial contact with a driving rate of 0.001 mm/s to bring the ball into contact with the surface of PZT specimen. At the same time, a 45 N (10 lb) load cell is used to measure and monitor the loading of specimen. The electric field was applied after the initial contact made. Following the period of system stabilization as defined above, the mechanical loading was applied with a displacement controlling mode at a rate of 0.01 mm/s.

The system designed and built in this stage of project is shown in Fig. 1. The transparent FC-40 fluid container is fixed on stage of indentation system. The container accommodates the ball-on-ring setup and components. Sealing is proven to be very effective to prevent the system from leaking, allowing the electromechanical testing to be done in a desired period.

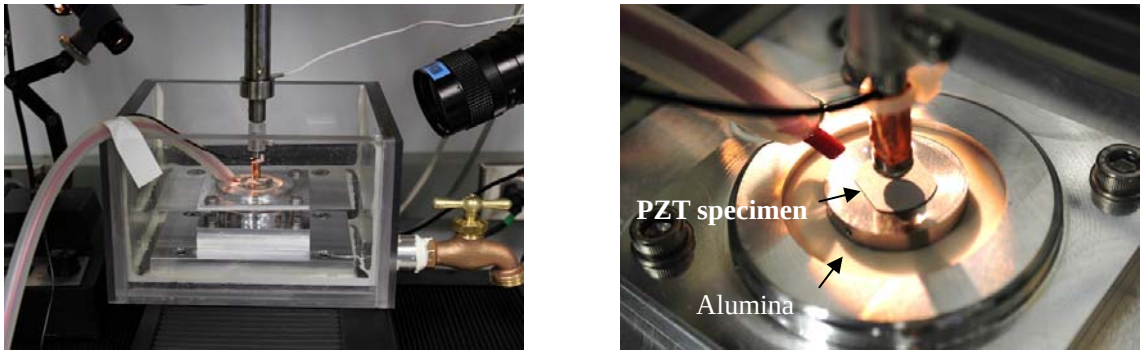

(a) (b)

Fig. 1 Ball-on-ring setup (a) general view with FC-40 container fixed on the stage of indentation system and (b) enlarged area showing PZT specimen, loading ball, and supporting ring that sits on an alumina disk.

The loading curve generally exhibited multiple peaks if the specimen was loaded all the way to the failure. The load corresponding to the first peak was taken as the failure load for estimating flexure strength. In several cases, the specimens were unloaded right after the first peak in order to preserve the fracture surface for subsequent fractography analysis.

Data on the flexure strength of poled KCI were collected in three different electric conditions: open circuit, +2Ec and -2Ec. Weibull plots for these three sets of data are given in Fig. 2(a). These plots are overlapped to a large extent. The data are also presented in terms of the confidence ratio rings at 95% confidence level in Fig. 2(b) along with those obtained with KCI specimens acquired in FY2009 (denoted as Y09). It can be observed that:

1) The effect of electronic fluid (FC-40) on the KCI flexure strength is statistically insignificant, given the same specimen state of PZT from two batches (Y09 and Y10),
2) Except the data set with –Ec, all data sets did not show statistically significant difference in their flexure strength.

The insensitivity of flexure strength for Y10 KCI on the electric field within the tested field range again demonstrated that the role of polarization as affected by the electric field did not influence the mechanical property in this case. This is corresponding consistently to the observation in Y09 KCI.

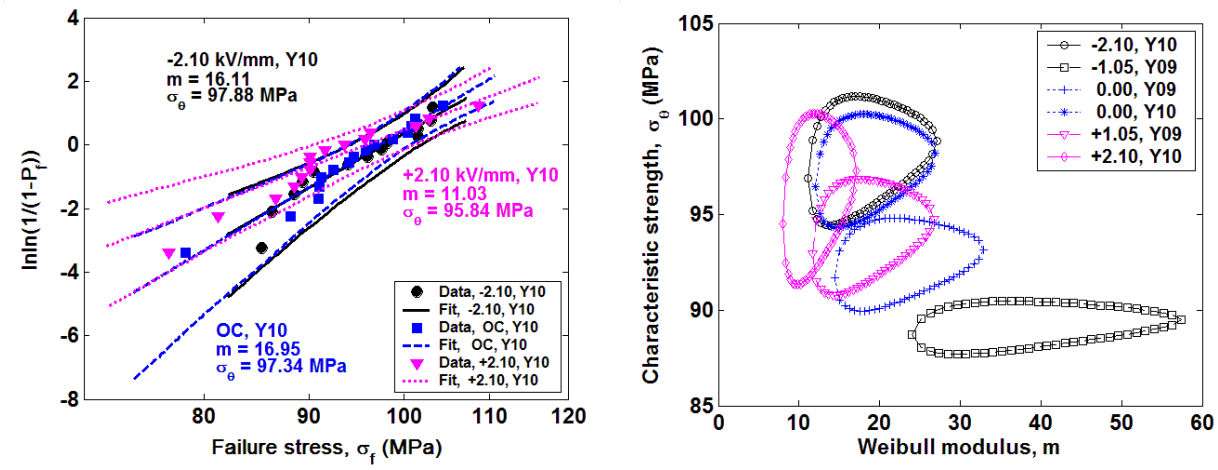

(a) (b)

Fig. 2 (a) Weibull plots for Y10 KCl specimens under open circle (OC), -2Ec (-2.1 kV/mm), and +2Ec (+2.1 kV/mm), and (b) confidence ratio rings of Y09 and Y10 specimens at 95% confidence level.

2. Mechanical Test and Characterization with Humidity

PZT stack in a fuel injection system is subjected to high humidity (~80%), in addition to high temperature and high electric field. Under extreme case, the water is attracted by the electric field and ionized by electrolysis.[1] Ag^+ ions move as Ag(OH) from the anode through cracks, voids, and defects to the cathode where they are recovered into metallic silver. This causes the silver dendrite to grow from the anode to the cathode resulting in the reduced resistance and dielectric breakdown. The degradation by humidity under an electric field was also observed for Pt electrodes as well. At the same time, it is well known that ceramics generally exhibit a subcritical crack growth dictated by the kinetics of reaction between the gaseous H_2O molecules and the stretched chemical bonding at the crack tip. Laag *et al*. showed that oxides such as alumina, zirconia, and PZT had a sharp drop of KIC near 2-10% RH (relative humidity).[2] Thus, moisture or water vapor plays an important role in the degradation of PZT materials and its effect on the mechanical strength and long-term reliability and lifetime of stacks needs to be carefully considered in designing PZT stack.

Study on the effect of relative humidity (RH) on the mechanical property of materials has been very active in the fields of historic material conservation, automotive paint systems, and polymer electrolyte membrane (PEM), etc. Foster *et. al*. investigated the effect of humidity on the mechanical property using dynamic mechanical analyzer (DMA).[3] The drive shaft operated vertically via a stand and a silicon washer provided seal between the glassware and the DMA measuring head. The glassware had a water jacket with an inlet and outlet port. Desired RH was achieved by mixing separate dry and 100% RH air

supplies regulated independently by 2 valves. A RH of 20 to 80% was obtained. A modified commercial chamber was used along with MTS Alliance RT/5 in studying PEM (Nafion). The environmental chamber from ESPEC Inc. delivered an environment of -70 to 170˚C and 30 to 95% RH.[4] Literature survey showed that, currently, the implementation of humidity in testing the mechanical properties of materials is mostly conducted case-to-case and no standard equipment is available.

The approach proposed under current consideration mainly consists of two procedures:

1) Pre-treat the PZT specimens in a controlled humidity chamber for a specific period of time (up to several thousand hours);
2) Transfer the treated specimen into a chamber that hosts the ball-on-ring setup, and perform the mechanical test.

The suggested approach shall simulate the long-term moisture attack and related damage event under piezoelectric loading. In addition, an environmental chamber with controlled humility capability will be designed and fabricated. The system will be used to determine the effect of a combined humility and electric field on the mechanical performance of PZT ceramics with and without thermal heat treatment (aging).

A number of EPCOS PZT stacks have been received recently through Cummins, Inc. These stacks are uncapsulated, and each of them was broken into 2 or 3 short stacks upon receiving of the stacks. Testing and characterization on these EPCOS stacks are being planned.

Status of FY 2010 Milestones

Measure and compare reliability of competing commercially available piezoactuators under consideration for use in diesel fuel injectors, *on schedule*.

Communications/Visits/Travel

Communications with Cummins, Inc. were made on CRADA update.

Publications/Presentations/Awards

1. Wang, H., Lin, H.-T., and Wereszczak, A. A., Strength properties of poled PZT subjected to biaxial flexural loading in high electric field, *J. Am. Ceram. Soc.*, 93 (9), 2010, 2843-2849.
2. Wang, H., Cooper, T. A., Lin, H.-T., and Wereszczak, A. A., Fatigue responses of PZT stacks under semi-bipolar electric cycling with mechanical preload, *J. Appl. Phys.*, 108 (8), 2010, 084107.

3. Wang, H., Matsunaga, T., Lin, H.-T., Mottern, A. M., and Wereszczak, A. A., Piezoelectric and dielectric performance of poled lead zirconate titanate in electric cyclic fatigue, in review
4. Wang, H., Matsunaga, T., and Lin, H.-T., Effects of temperature and electric field on mechanical strength of single-layer PZT plate, in preparation.

References

1. P. Pertsch, S. Richter, D. Kopsch, N. Kramer, J. Pogodzik, and E. Hennig, Reliability of piezoelectric multilayer actuators, ACTUATOR 2006 Conference, Bremen, Germany, Jun14-16, 2006
2. N. J. van der Laag, L. J. M. G. Dortmans, and G. de With, Influence of relative humidity on mechanical properties of alumina, PZT and Zirconia, Key Engineering Materials, 206-213, 751-754 (2001).
3. G. M. Foster, S. Ritchie, and C. Lowe, Controlled temperature and relative humidity dynamic mechanical analysis of paint films, J. Thermal Anal. Calorimetry, 73, 119-126 (2003).
4. Y. Tang, A. M. Karlsson, M. H. Santare, M. Gilbert, S. Cleghorn, and W. B. Johnson, An experimental investigation of humidity and temperature effects on the mechanical properties of perfluorosulfonic acid membrane, Mater. Sci. Eng. A, 425, 297-304 (2006).

Agreement 15050: Evaluation of Materials via ACERT Engine

Michael Kass, Brian Kaul, Norberto Domingo, Robert M. Wagner,
K. Dean Edwards, H. T. Lin, and D. Ray Johnson
Oak Ridge National Laboratory

Objective/Scope

This project is focused on improving the performance, emissions and efficiency of heavy-duty diesel engines through the application of materials enabled technologies. The range of material systems is comprehensive and includes 1) improved structural materials to accommodate higher cylinder pressures and temperatures, 2) improved durability and corrosion resistance, 3) low inertial components to improve transient response, 4) improved emissions control performance, and 5) waste heat recovery systems.

To date a dynamometer engine research cell was constructed for use with heavy-duty engines. A 2004 C15 ACERT Caterpillar engine was provided by the Caterpillar materials research staff for materials-based efficiency evaluations. The engine was instrumented for combustion and thermal assessment. During FY09, the engine performance was assessed according to thermal availability and opportunities for efficiency improvements were identified. ORNL also completed a WFO with Caterpillar to evaluate a novel turbo concept. The novel turbo design was found to deliver efficiency and thermal improvements over the baseline turbo design. At the conclusion of these efforts, several materials-related efficiency improvement concepts were discussed and debated. The decision was to consider advanced alloy utilization in key components and emission control technologies.

Progress This Quarter (October – December 2010)

Several projects were proposed for FY2011; they include valve material durability and high temperature exhaust manifold performance. Caterpillar has provided ORNL with a set of valves that composed of a novel high temperature nickel-based alloy for improved durability. The valves durability study was started on January 27 of 2011. For this study, the engine is to be run for 200 hours according to the transient cycle shown in Fig. 1. The transient cycle consists of several high load settings and idle engine operation. In addition the valve lash was measured for the untested condition and after 25 and 50 hours of engine operation. The lash results are shown in Fig. 2 and indicate that the valve recession for those composed of the nickel-based alloy are identical to the lash measurements obtained for the standard valves. Upon completion of the 200 hour run, the valves will be removed and the valve performance will be evaluated by a team of materials researchers from ORNL and Caterpillar.

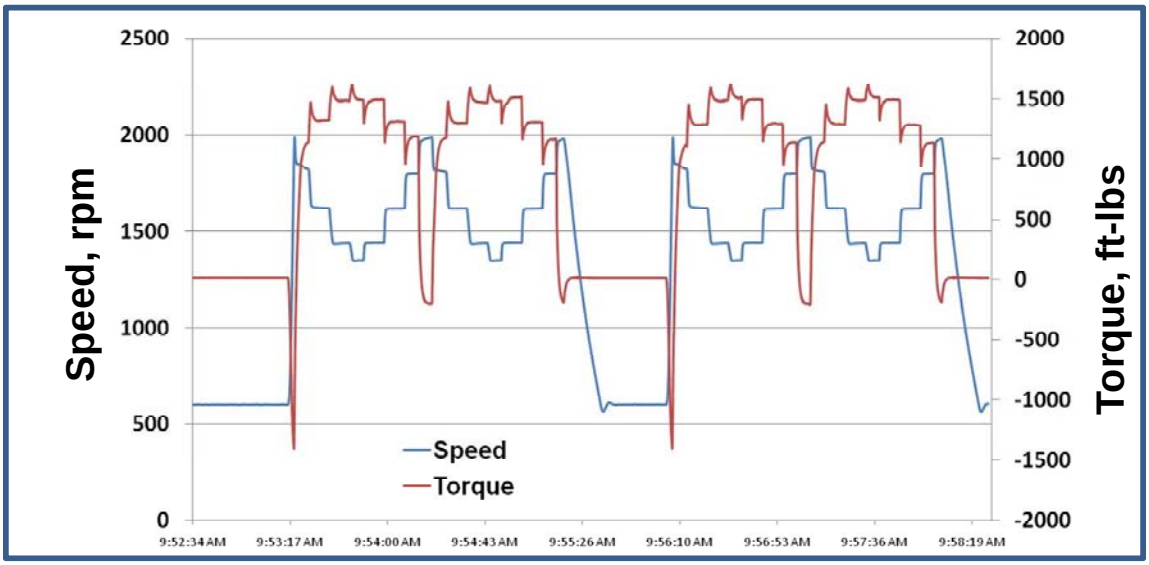

Fig. 1. Schematic of transient test cycles used to evaluate valve performance.

Table 1. Valve lash measurements for each valve as a function of operating time

Cylinder Number	Valve Material	Valve Number	Time of Exposure		
			0 hours	30 hours	50 hours
1	Ni alloy	1	0.030	0.028	0.028
		3	0.030	0.028	0.028
2	Standard	5	0.030	0.028	0.028
		7	0.030	0.028	0.028
3	Ni alloy	9	0.030	0.028	0.028
		11	0.030	0.028	0.028
4	Standard	13	0.030	0.028	0.027
		15	0.030	0.028	0.027
5	Ni alloy	17	0.030	0.029	0.028
		19	0.030	0.028	0.028
6	Standard	21	0.030	0.028	0.027
		23	0.030	0.028	0.027

Publications/Presentations/Awards

None reported during this quarterly period.

Plans for Next Reporting Period

- Complete engine evaluation for novel valve materials.

Agreement 16303: Materials for High Pressure Fuel Injection Systems

Peter J. Blau and Amit Shyam
Oak Ridge National Laboratory
and
Nan Yang
Caterpillar Corporation

Objective/Scope

The objective of this Cooperative Research and Development Agreement (CRADA) between UT-Battelle, LLC and Caterpillar Corporation is to advance the state of the art in the characterization, selection, and use of metallic alloys for high-pressure diesel engine fuel injector nozzles.

During recent decades, fuel efficient, low-emissions diesel engine designs for heavy trucks have relied upon increasing fuel injection pressures to optimize combustion characteristics. Precise fuel metering is required. This key functional requirement has raised concerns over the ability of spray holes to be machined to sufficiently close tolerances to provide desired spray patterns and for the materials of construction to withstand hundreds of millions of high-pressure pulses without succumbing to fatigue damage. The data and analyses obtained in the course of this three-year effort are expected to provide vital information for designers and material selectors for high-performance fuel systems for energy-efficient diesel engines.

A three-pronged approach has been developed. It involves: (1) characterization of current fuel injector hole geometry and alloy metallurgy, (2) measuring the residual stress in nozzle tips near spray holes, and (3) development and use of specialized fatigue test methods to address the special requirements of the next generation of high-pressure fuel injectors.

Technical Highlights

*Fatigue testing on fuel injector materials***.** A dual-pronged approach for characterizing the effects of small holes on the fatigue life and crack growth mechanisms of fuel injector alloys is being implemented. The first approach is to conduct axial-fatigue tests on smooth specimens without holes. A summary of the smooth specimen stress life behavior of a tool steel having a composition used in high-pressure fuel injectors, and with two different heat treatments, is summarized in Figure 1. These data demonstrate that heat treatment can have a significant effect on the fatigue life of fuel injector tip materials. Initial results show as much as a 20% reduction in life for one heat treatment compared with another. The same approach has been implemented to discern the crack initiation mechanisms that operate over a range of applied loads. Some failures were seen to initiate from surface flaws and others subsurface flaws.

The second approach is to conduct a fracture mechanics characterization of cracks initiating and propagating from artificial defects machined on both axial and bending specimens. The artificial defects were fabricated by electro-discharge machining (EDM) to approximate dimensions of a spray hole in a fuel injector tip.

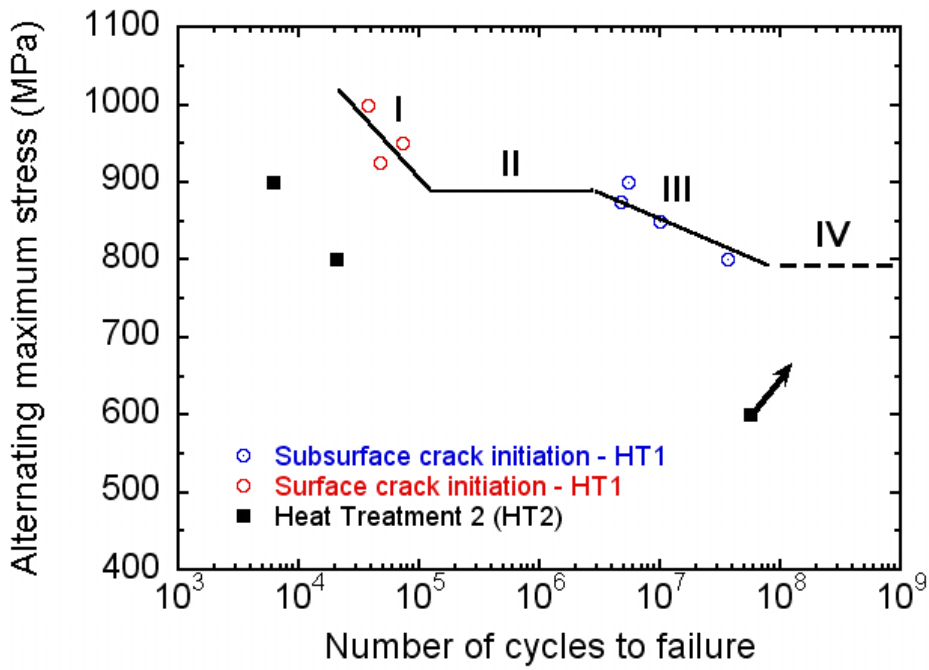

Figure 1. The effect of heat treatment on SN-behavior of a tool steel alloy. A heat treatment alone can modify the endurance limit of the alloy by more than 200 MPa.

An example of an artificial defect, showing a fatigue crack initiating and propagating from it, is shown in Figure 2. Some of the tests have been run for more than ten million cycles. To develop a better understanding of the range in material properties for low and high loads, fatigue crack propagation curves were determined for specimens such as this under various experimental conditions.

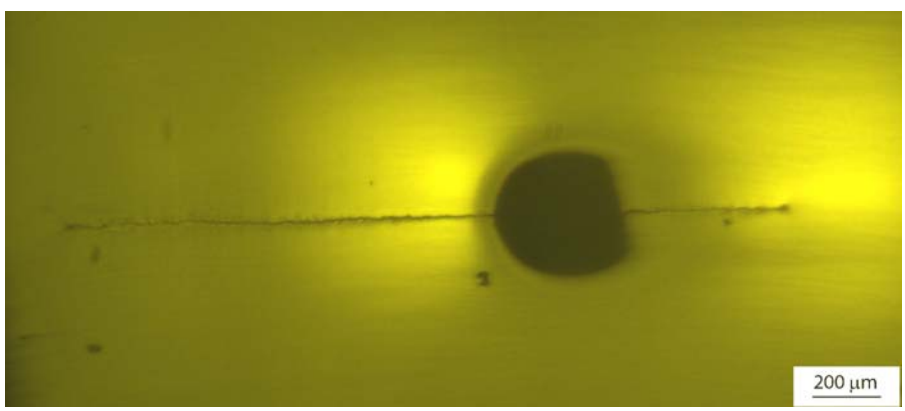

Figure 2. Image of a fatigue crack that is emanating from an EDM notch at a maximum stress of 800 MPa and R = -1. The testing conditions including the geometry of the EDM hole simulate the loading conditions observed in a diesel fuel injector during service.

In addition to the work presented in Figure 2, fatigue crack propagation thresholds were determined for the small cracks by modifying the procedure available for long fatigue cracks in the standard ASTM E647-05. The generated experimental information can be applied to implement a damage tolerant design for fuel injector materials.

Plans for the Next Quarter

1) Continue to investigate the axial fatigue life and fatigue crack propagation behavior for fuel injector steels.

2) Conduct nano-indentation hardness studies of the material surrounding the walls of injector spray holes.

3) Plan experiments to investigate the effects of diesel fuel environment on smooth specimen axial fatigue failures.

Status of FY 2011 Milestones

1) Complete baseline fatigue tests on smooth specimens without artificial flaws. **(3/31/2011) Status:** extended from 2010 to 3/31/2011 due to a delay in receiving heat-treated test specimens.

2) Complete fatigue tests on steel specimens containing EDM holes in the presence of diesel fuel and prepare a final report. **(9/30/2011) Status**: on-going.

Communications/Visits/Travel

Dr. Nan Yang from Caterpillar will visit ORNL in March 2011 to solidify plans for the remainder of this project.

Problems Encountered

Assignment of a new principal investigator by the CRADA partner momentarily interrupted the continuity of the project, but conference calls and a meeting of the project team at ORNL during the coming quarter will bring the team up to speed for the final phases of the effort.

Publications/Presentations/Awards

A. Shyam, P. J. Blau, and M. J. Pollard "The very high cycle fatigue behavior of tool steel materials for diesel fuel injectors," accepted for the 5th International Conference on Very High Cycle Fatigue, Berlin, Germany, June 28-July 1, 2011.

References

None

Agreement 16304: Materials for Advanced Engine Valve Train

P.J. Maziasz, and N.D. Evans
Oak Ridge National Laboratory
and
M.D. Veliz
Caterpillar, Inc.

Objective/Scope

This is an ORNL CRADA project with Caterpillar, NFE-07-00995 and DOE OVT Agreement 16304, which was extended for 24 months last year, and is now scheduled to end in Dec., 2012. This CRADA project focused on addressing the wear and failure modes of current on-highway heavy-duty diesel exhaust valves and seats, and then evaluating changes in valve-seat design or the selection of advanced alloys, which will then enable higher temperature capability, as well as better performance and durability. Requests for more detailed information on this project should be directed to Caterpillar, Inc.

Highlights

Caterpillar, Inc.

Caterpillar completed wear-rig testing very high temperature wear-rig tests of new prototype exhaust valves made from upgrade Ni-based superalloys with higher temperature capability than standard 31V superalloy valves. Additional testing based on these results is planned.

ORNL

ORNL has completed some of the initial creep-rupture testing at 816°C and above of specimens from the same upgrade Ni-based superalloys used to make new prototype exhaust valves for testing at Caterpillar. Both Ni-based alloys 1 and 2 show higher temperature capability and performance compared to the standard 31V superalloy.

Technical Progress, 1st Quarter, FY2011

Background

This OVT Agreement 16304 is an ongoing ORNL CRADA project with Caterpillar, NFE-07-00995, which will last for about 5.5 years, after last year's new 24 month extension. This CRADA project has addressed the wear and failure modes found for current on-highway heavy-duty diesel exhaust valves and seats. It then identified changes in valve-seat advanced alloys that will enable higher temperature capability, as well as better performance and durability. The need for such upgraded valve-seat alloys is driven by the demands to meet new emissions and fuel economy goals, which continue to push diesel exhaust component temperature higher. The CRADA was extended for 24 more months due to outstanding technical progress and success at mitigating wear between exhaust valves and seat-inserts at above 800°C.

Requests for more detailed information on this project should be directed to Caterpillar, Inc.

Approach

Caterpillar provides the baseline wear and mechanical behavior characteristics of engine-exposed standard valves and seats, and provides exposure of similar components from simulation-rig testing at Caterpillar. ORNL provides more in-depth characterization and microcharacterization of those valves and seats, and provides knowledge and understanding of the full range of commercially available heat-resistant alloys, to select those most suitable for upgraded valve performance. ORNL and Caterpillar have developed an understanding of the underlying degradation mechanisms, which is the technical basis for selecting and testing alternate valve and seat alloys with upgraded performance and temperature capability. Caterpillar and ORNL are working with Caterpillar's various component and materials suppliers, to enable prototype production of upgraded exhaust valves and seats for evaluation in Caterpillar's wear-test rig, and parallel testing and characterization of the same advanced alloys at ORNL.

Technical Progress – Caterpillar, Inc.

Caterpillar previously obtained from a major valve supplier two heats of advanced, alternate Ni-based superalloys for forging into upgraded exhaust valves. These new upgrade Ni-based alloys should have improved performance and higher temperature capability than the standard 31V alloy. This quarter, Caterpillar completed some of the initial testing and evaluation of Ni-based 1 and 2 alloys in the wear-test rigs. The improvement in seat-valve wear at 850°C for Ni-based alloy 1 relative to the standard production 31V alloy is nearly 200%, as shown in Figure 1. Additional wear-rig testing of Ni-based alloys 1 and 2 is planned, and characterization at both Caterpillar and ORNL are in progress for tests that are complete.

Technical Progress – ORNL

ORNL previously obtained new forged valves and various mechanical properties test specimens from one of Caterpillar's exhaust valve suppliers of two alternate alloys, Ni-based 1 and 2. Both Ni-based alloys have more temperature capability and performance than the standard 31V alloy. Previously it was shown that both alternate Ni-based alloys have higher tensile yield strength (YS) of 90-100 ksi when tested at 816°C (1500°F) in the age-hardened condition with no service, compared to the YS of about 70 ksi for the standard 31V alloy. Creep-rupture testing began previously, and the initial tests run at 816°C and 30 ksi (207 MPa) were completed this quarter, as shown in Figure 2. While both Ni-based alloys 1 and 2 have much better creep-resistance than standard 31V, Ni-based alloy 1 has significantly more creep-resistance than Ni-based alloy 2. The differences between the various alloys after creep-rupture testing are much larger than their differences after tensile testing. Creep-testing at 816 and 871°C will continue next quarter.

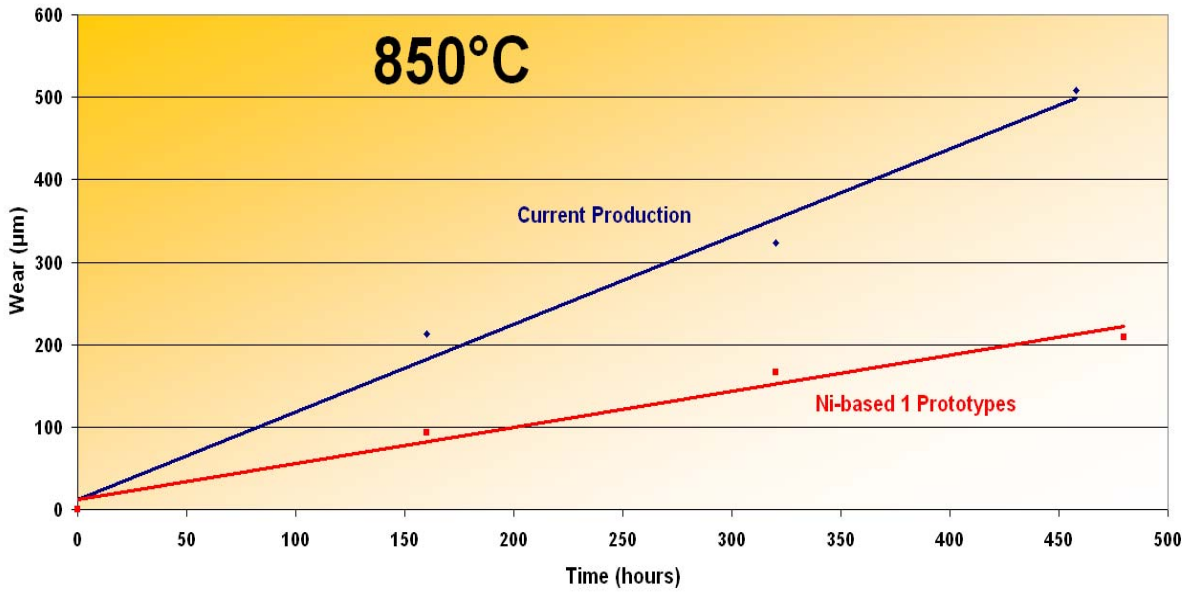

Figure 1**.** Caterpillar wear-rig testing of cumulative wear (valve and seat-insert) for standard 31V alloy exhaust valves and new Ni-based 1 superalloy prototype valves at 850°C in air. The Ni-based 1 alloy showed a 200% reduction in wear relative to the 31V alloy.

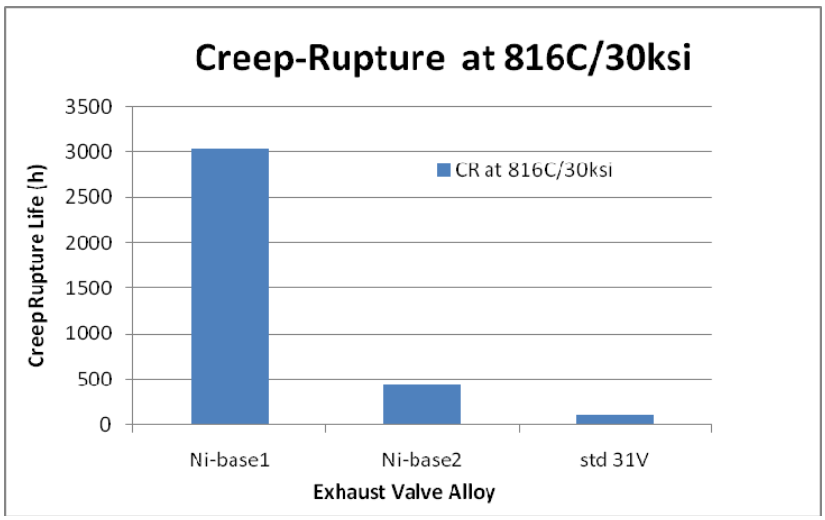

Figure 2. Creep-rupture life of the standard 31V exhaust valve alloy and two alternate upgrade Ni-based superalloys, for creep tests run in air at 816°C (1500°F) and 30 ksi (207 MPa).

Tensile/creep specimens of these alloys are also being aged in this same temperature range of 816 to 871°C, and aging to about 5000 h should be completed next quarter. Microcharacterization of the rig-tested valves from Caterpillar began this quarter and will continue next quarter.

Communications/Visits/Travel

Detailed team communications between ORNL and Caterpillar occur regularly in multi-party conference calls. Caterpillar has extended team discussions to include their commercial seat-insert supplier as well as one of their exhaust valve suppliers. Mark Veliz from Caterpillar visited ORNL in November, 2010 to review and discuss details of this project

Status of Milestones (ORNL for DOE)

Milestone for Caterpillar rig-testing of prototype valves and seats of new advanced alloys (Nov., 2010) was completed this quarter. Milestone for completing initial creep-rupture testing of new Ni-based superalloys with upgraded performance at ORNL is on schedule for FY2011.

Publications/Presentations/Awards

None

Agreement 17257: Materials for Advanced Turbocharger Designs

P.J. Maziasz and A. Shyam
Oak Ridge National Laboratory
and
K. Pattabiraman
Honeywell Turbo Technologies

Objective/Scope

This ORNL CRADA project with Honeywell, NFE-08-01671 (DOE/EERE/OVT Agreement 17257) began last year, and is scheduled to last for about 3 years. This CRADA project addresses the limitations of lifetime or use-temperature for the various components (casing, wheel, shaft, bearings) of both the turbine and compressor parts of the turbocharger system. As exhaust temperatures increase, to provide higher engine efficiency and lower emissions, turbocharger component temperatures also increase, so the need for more heat-resistant materials must be addressed. Requests for more detailed information on this CRADA project should be directed to Honeywell, Inc.

Highlights

Neutron-scattering experiments at ORNL to measure residual-stresses in critical locations of wheel/shaft assemblies and turbine housings began this quarter. Long-term creep-testing of cast CF8C-Plus austenitic stainless steel at 600°C continued this quarter. Assessments of the oxidation-resistance of CF8C-Plus steel relative to other exhaust component cast-irons and steels began this quarter.

Technical Progress, 1st Quarter, FY2011

Background

This CRADA project began last year, and will extend for 3 years, and covers several different tasks. The first task was to assess and prioritize the various components that need or would most benefit from materials upgrades to increase temperature capability and performance, as well as durability and reliability. The next tasks examine current performance and degradation modes of wheel/shaft assemblies for turbines and compressors, housings for turbines and compressors, and bearings. These tasks may then obtain and test new materials with upgraded performance, and provide the results to Honeywell for designing advanced turbocharger systems, or manufacturing of new prototype components for testing and evaluation.

Approach

This CRADA project began early last year. This project is comprised of six tasks, which will span the next 36 month period. Activity began with ORNL and Honeywell discussing the priority of the various turbocharger components for materials upgrades. A turbocharger system includes the hot (turbine) end, driven by exhaust gas from the engine, a cold (compressor) end to increase air pressure into the combustion changer, and a transition region that connects these two ends. The turbine and compressor wheels are connected to a common shaft, supported by bearings. For the first task, the

turbine wheel-shaft assembly was chosen as the first component for consideration, with analysis focused on residual stresses near the weld-joint of the Ni-based superalloy wheel to the steel shaft, which can upset balance during service. Another task of this new CRADA project continues previous work between ORNL and Honeywell on testing of the new CF8C-Plus cast stainless steel as a significant performance upgrade for the turbine housings relative to standard SiMo or Ni-resist cast irons. This CRADA project for turbine housings covers a broad range of other high temperature properties, including creep and fatigue strength, and includes turbine housing applications for passenger vehicle gasoline engines.

Technical Progress

For Task 1, Honeywell identified neutron-scattering experiments to measure residual stresses in welded wheel/shaft assemblies as one of their highest priority items. For Task 2, these experiments were defined, and the proposal needed to obtain neutron scattering time at the HFIR Residual Stress User- Facility, was completed this quarter. Figure 1 shows a typical Honeywell wheel/shaft assembly. Preliminary neutron-scattering experiments for diffraction analysis of the steel shaft were completed this quarter as well.

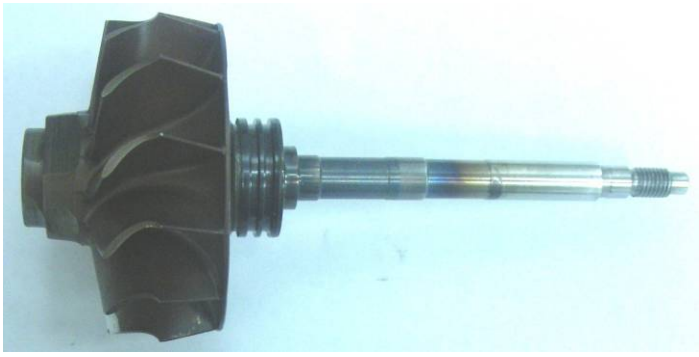

Figure 1 – Honeywell turbocharger wheel/shaft assembly, consisting of a Ni-based superalloy turbine wheel welded to a steel shaft.

For Task 3, ORNL continued long-term creep-rupture tests at 600°C of the cast CF8C-Plus stainless steel this quarter, which began previous. ORNL began aging of as-cast CF8C-Plus tensile/creep specimens at 700 and 800°C last quarter, which will continue this quarter. ORNL also identified additional longer-term creep-rupture testing at 700-800°C that will add to previous creep-rupture data on CF8C-Plus and HK30-Nb steels, which will begin this quarter. Honeywell continued to address the next steps necessary to commercially produce some prototype turbocharger housing using CF8C-Plus steel for certain turbocharger models, so that they could be evaluated and tested on engines.

Oxidation experiments to assess the oxidation-resistance of cast CF8C-Plus relative to several cast-irons used for conventional turbochargers and exhaust system components began this quarter, and will continue next quarter.

Communications/Visits/Travel

Periodic conference calls are held between ORNL and Honeywell Turbo Technologies, and email communications help to coordinate the work

Status of Milestones (ORNL for DOE)

The FY2011 milestone to begin initial neutron-scattering residual-stress measurements on wheel/shaft assemblies for turbochargers (12/2011) was achieved, and the other milestones for FY2011 are on-track.

Publications/Presentations/Awards

None

Agreement 17894: NDE for ACERT Engine Components

J. G. Sun and Mark Veliz*

Argonne National Laboratory

***Caterpillar, Inc.**
Technical Center

Objective/Scope

Applications of advanced materials in diesel engines may enhance combustion and reduce parasitic and thermal losses, thereby improving engine efficiency. Engine components developed from advanced materials, however, require rigorous assessment to assure their reliability and durability in more stringent operating conditions. The objective of this work is to develop and assess various nondestructive evaluation (NDE) methods for characterization of advanced engine components in a Caterpillar heavy-duty ACERT experimental engine at ORNL. NDE technologies established at ANL, including optical scanning, infrared thermal imaging, ultrasonics, and X-ray computed tomography (CT), will be further developed for detection of volumetric, planar, and other types of flaws that may limit the performance of these components. NDE development will be focused on achieving higher spatial resolution and detection sensitivity. Current efforts are directed in applications of optical methods for valvetrain components, X-ray and ultrasonic for joinings, and thermal imaging for thermal barrier coatings (TBC).

Technical Highlights

Work during this period (October-December 2010) focused on synchrotron X-ray CT characterization of friction-welded joints between TiAl turbine wheel and Ti-6Al-4V shaft and on thermal tomography development for high-resolution imaging of TBCs.

1. Synchrotron X-Ray CT Characterization of Joints

Friction welding to join TiAl turbine wheel and Ti-6Al-4V shaft has been investigated by Caterpillar for many years [Yang et al, 2005], see Fig. 1. In early trials, cracking at the joint plane was one of the main technical challenges. With process improvements, crack-free joints with tensile strength higher than the base TiAl material can be routinely produced. However, the variation of material properties in the parts from different supplies may alter the processing condition and generate cracking within the joints. In an industrial setting, weld inspection is usually conducted using ultrasonic NDE method because of its low cost and high speed. However, ultrasonic signal can be difficult to interpret, especially for complex samples like friction-welded joints. As a result, detailed calibration of ultrasonic data with flaw geometry, usually obtained from destructive examinations, has to be performed to qualify the use of ultrasonic method. This calibration, however, may not be always possible because it is not feasible to conduct destructive examination for all potential flaws. X-ray CT method, which can generate 3D image of the inspected part, is suitable for nondestructive determination of the 3D flaw geometry that can be used as the basis to qualify the ultrasonic method. The detailed 3D data may also help to understand the effect of various processing parameters to the weld quality, which may lead to process optimization to produce reliable components. The requirement for X-ray imaging of the friction-welded joints includes high spatial

resolution and high X-ray energy to penetrate the part. Synchrotron X-ray CT meets these requirements and is the ideal method to evaluate these joints.

Beside synchrotron X-ray CT, an industrial X-ray CT system within our NDE group was also investigated. The system consists of a 450 kV X-ray source and a line detector with 80 µm pixel-size sensors and a large-panel area detector with 200µm pixel size. Three friction-welded joints were evaluated, one cut sample shown in Fig. 1b and two complete samples similar to those in Fig. 1a. Weld cracks in the cut sample can be analyzed from the optical micrograph as shown in Fig. 2. The cracks are extended more than one-half of the width of the shaft wall. The crack gap is very narrow, especially near the tip. Figure 3 shows enhanced digital radiographs of this cut sample and another un-cut sample. The weld cracks in both samples are detected, although the detected crack lengths are shorter than that observed in the micrograph because of the low spatial resolution of the area X-ray detector (200 µm). Higher-resolution CT slicing was also tried using the line detector (80 µm); results were not satisfactory because of insufficient resolution as well as low X-ray intensity (flux) which reduced the signal-to-noise ratio.

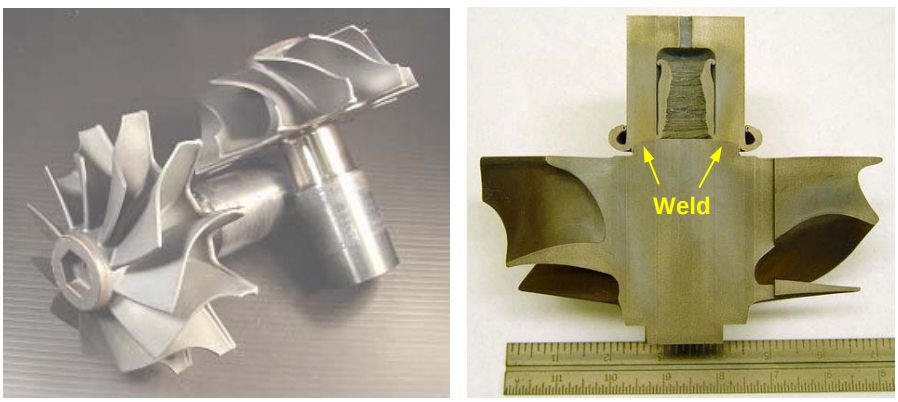

(a) (b)

Fig. 1. Friction-welded turbine wheels: (a) from Yang at el [2005] and (b) a cut sample.

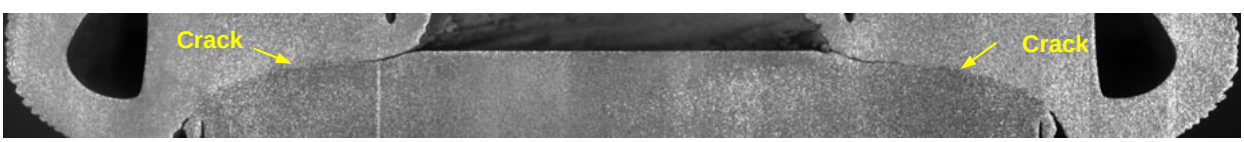

Fig. 2. Optical micrograph of the cut surface of the cut sample in Fig. 1b.

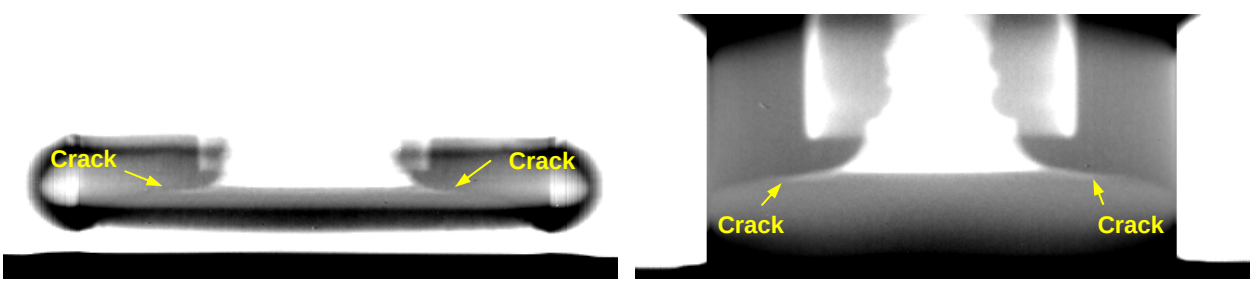

(a) (b)

Fig. 3. Digital radiographs of a (a) cut and (b) complete friction-welded joint samples.

High-energy synchrotron X-ray CT, developed at the advanced photon source (APS) at ANL, was found to be suitable for NDE characterization of the joint quality. The synchrotron X-ray source has high peak energy (>250 keV) to penetrate the metallic material, and the detector (imager) has a high spatial resolution (~40 µm) to resolve small flaws. An earlier test was conducted for calibration joint samples shown in Figs. 1-3 (they contain weld cracks). A new test was conducted in this period to investigate the weld quality as well as to detect casting flaws within a TiAl wheel cast. Preliminary results for the calibration samples are analyzed and discussed in this report.

Figure 4 is a typical cross-section CT slice of the cut sample as shown in Fig. 1b (the image voxle size is 43.7 µm). This slice passes through the weld plane: the internal area belongs to the TiAl cast wheel and the external region to the Ti-alloy shaft. The crack between the two materials is shown as the darker semicircle of irregular shape, with some small voids inside the crack line (within TiAl). All cross-section slices acquired for this sample, total of 140 slices, were then composed together and sliced in the axial direction for a better visualization of the cracks. Figure 5 shows the reconstructed axial slice at the cut surface of the sample; i.e., it is at the same axial plane as the optical image in Fig. 2. This axial slice shows 7 segments along the axial direction because 7 scans were performed to cover the axial length (each scan for ~0.7 mm length). By comparing the images in Figs. 2 and 5, the CT image shows a better contrast of the welding crack. The detailed crack dimension (length) can be easily determined, as shown in Fig. 6. The crack dimensions determined from the CT image are similar to those observed in the micrographs, indicating that the CT spatial resolution is adequate to resolve such welding cracks.

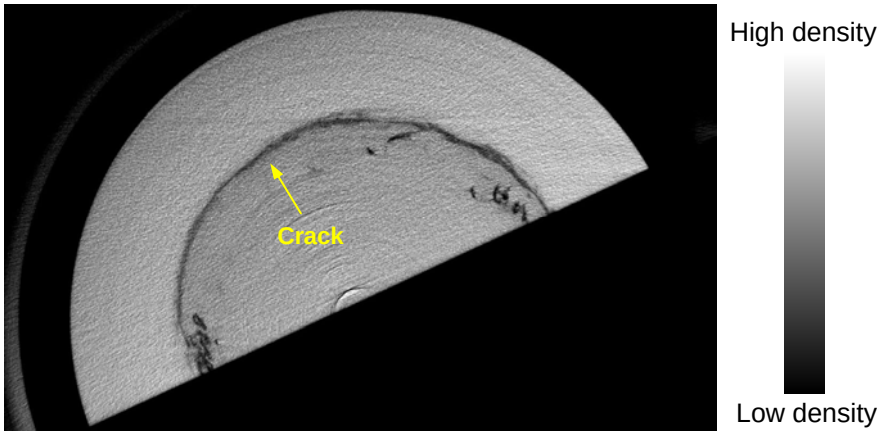

Fig. 4. A typical X-ray CT slice within weld plane of the cut sample shown in Fig. 1b.

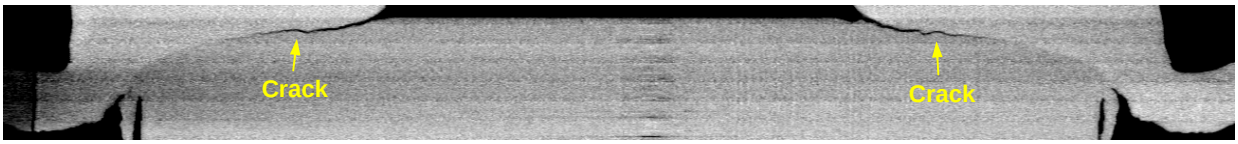

Fig. 5. Axial slice near cut edge as viewed in Fig. 2 for cut sample shown in Fig. 1b.

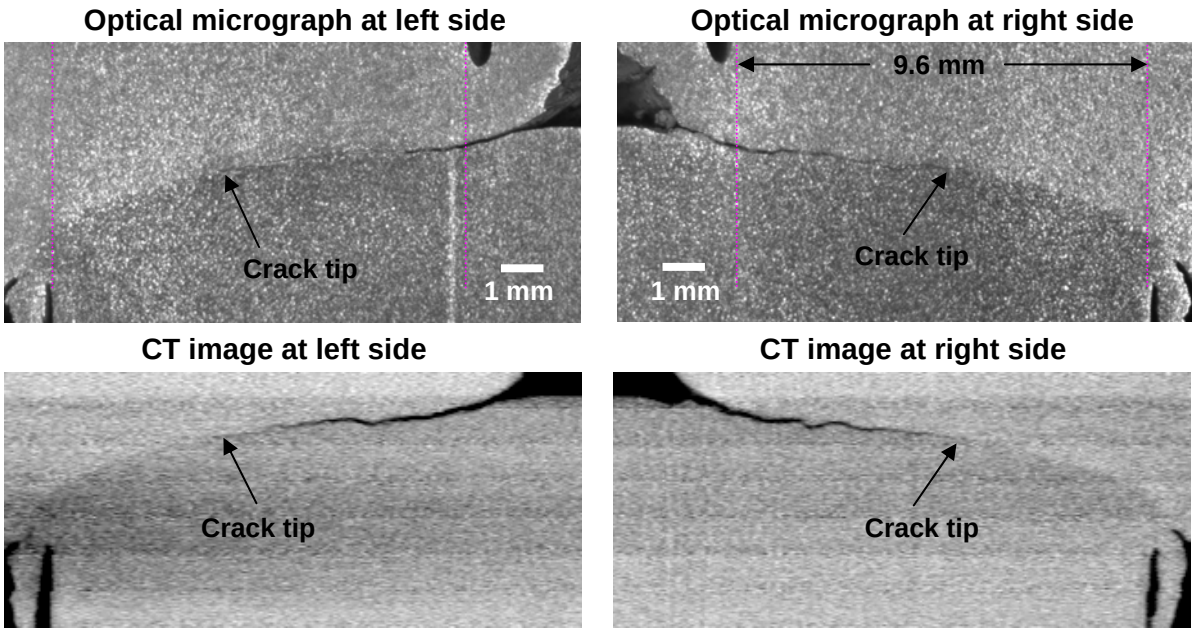

Fig. 6. Detailed comparison of optical and CT images at the cut edge of cut sample shown in Fig. 1b.

Figure 7 is a typical cross-section CT slice of a complete joint sample. This slice passes through the joint plane, with the welding crack shown as the darker circle of irregular shape. It is apparent that the crack has a complex structure that could be related to processing parameters. If a relationship between the crack structure at the joint plane and processing parameters is determined, it could be used to optimize the friction-welding process to produce reliable joints. In Fig. 8, a typical reconstructed axial slice is presented, which also shows complex crack geometry at the joint plane.

Figure 9 shows two cross-sectional CT slices of another complete joint sample. These slices are within the TiAl cast, located at 4.1 and 1.5 mm away from the joint plane, and they show axial cracks inside the cast. This sample has been inspected using ultrasound at Caterpillar, and the result indicated some flaws within the sample. However, ultrasonic result could not identify the flaw types as well as the exact location and the size of the flaws. The CT slice images in Fig. 9 show clearly the axial cracks inside the TiAl cast. In Fig. 9a, the slice at 4.1 mm away from the joint plane, the cracks are barely seen so are the tips of the cracks (which give the approximate depth of the cracks). In Fig. 9b, the geometry and the length of the cracks are well defined. Such detailed information about the crack geometry may be used to calibrate the ultrasonic inspection so an accurate interpretation of the ultrasonic results is possible. This is important for quality control in manufacturing facilities because only ultrasonic technique can be used in such environment. This calibration will be attempted in the next reporting period using the ultrasonic system at ANL.

The slice images in Figs. 7 and 9 also show the ring artifact which appears as the darker/brighter semicircles that are more prominent near centers. This artifact is due to the sensitivity variation of the individual X-ray sensors during the X-ray scan period.

This artifact has been found to be more severe in the experimental data acquired in this period. Although it cannot be removed completely, additional image processing may reduce the effect. Such improvement may also help for better resolution of cracks and the interface between TiAl and Ti-alloy (which have similar density so a small X-ray contrast between them). Development of data-processing algorithms will be conducted in the next period.

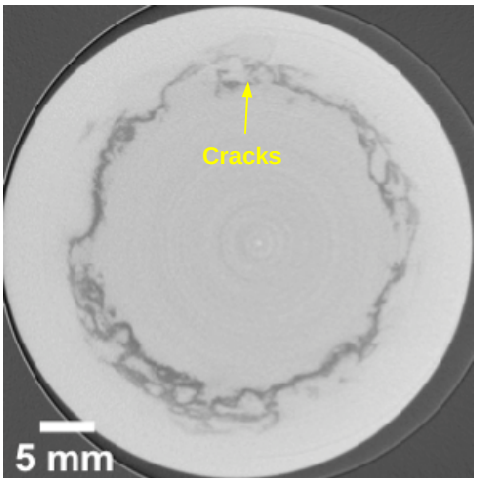

Fig. 7. A typical X-ray CT slice within weld plane of a complete sample.

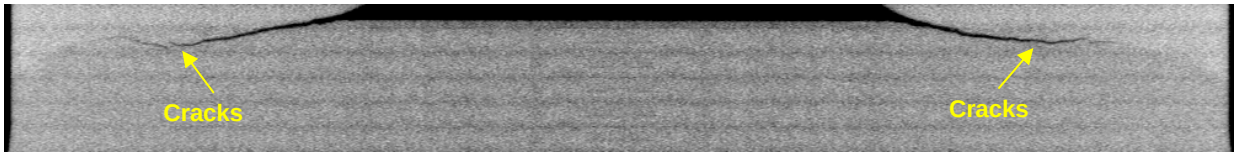

Fig. 8. Reconstructed axial slice image for the same complete sample as in Fig. 7.

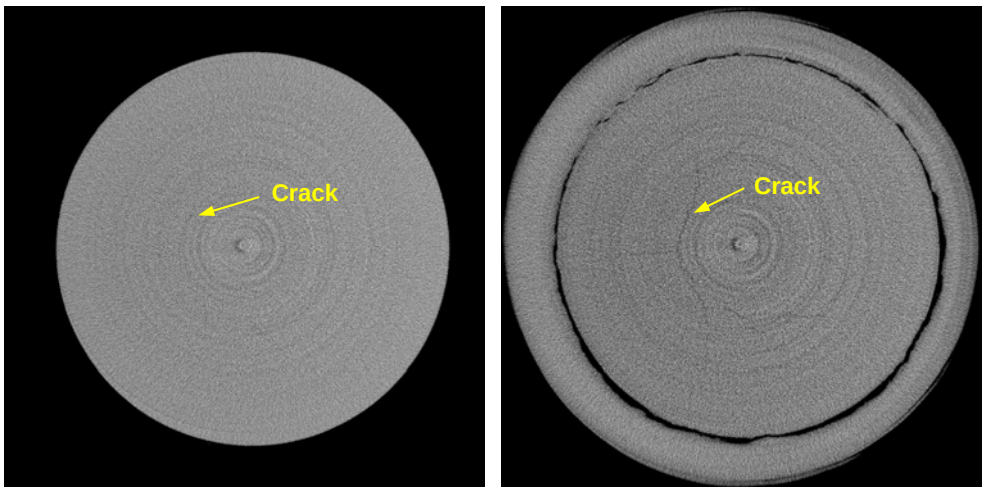

(a) (b)

Fig. 9. X-ray CT slices within TiAl cast located at (a) 4.1 and (b) 1.5 mm away from the weld plane of another complete sample.

2. High-Resolution Imaging of Thermal Barrier Coatings by Thermal Tomography
With drastic increases in fuel standard being proposed recently at the state and federal levels, advanced materials such as TBCs become necessary to achieve the goals. Material characterization methods, such as NDE methods, will be essential for the materials development. During this period we continued the development of the thermal tomography method for high-resolution imaging of TBCs. It was identified that a high lateral resolution requires hardware modification and a high depth resolution requires software development. Progress in these directions will be reported in future reports.

References

Nan Yang, et al., "Development of Titanium Alloys for Heavy-Duty Diesel Engines," Quarterly Progress Report for April through June 2005, Heavy Vehicle Propulsion Materials Program.

Status of Milestones

Current ANL milestones are on schedule.

Communications/Visits/Travel

J.G. Sun visited Caterpillar on Nov. 18, 2010 to discuss project issues.

J. G. Sun plans to present a paper entitled "Thermal Imaging Measurement Accuracy for Thermal Properties of Thermal Barrier Coatings" and an oral talk on "Nondestructive Evaluation of Ceramic Materials by Thermal Tomography" at the 35th International Conference and Exposition on Advanced Ceramics and Composites, Daytona Beach, FL, January 23-28, 2011.

Problems Encountered

None this period.

Publications

None this period.

Agreement 18570: Engine Materials Compatibility with Alternate Fuels

S. J. Pawel
Oak Ridge National Laboratory

Objective/Scope

The purpose of this Cooperative Research and Development Agreement (CRADA) between Oak Ridge National Laboratory and USCAR is to systematically evaluate compatibility between engine materials and ethanol fuel blends over a range of temperatures consistent with engine operation. Four primary tasks are included in the overall program:

1) surface analysis of materials exposed in field and lab exposures
2) in-situ extraction of gas and/or fluid from the valve seat crevice
3) development of electrochemical testing protocols
4) laboratory corrosion exposures of coupon materials

Technical Highlights

Emphasis in the first quarter of FY11 revolved around initiation of corrosion testing of aluminum alloys suitable for engine applications (associated primarily with Task 4, with relevance to Task 3). Corrosion testing in alternate fuels was initiated using cast alloys 319, 333, and 356 as well as wrought alloy 1100 (all purchased from a specimen shop) and more recently the USCAR Partners were able to provide seven additional cast aluminum alloys of interest (designated alloys A through G at present) to incorporate into the test program.

Initial testing included static exposures of alloys 319, 333, 356, and 1100 in CE50a and CE85a at 90°C for one week in a Teflon-lined autoclave. Specimens were fitted with a crevice washer to aggravate localized corrosion tendencies. The designations CE50a and CE85a indicate E50 and E85 solutions to which a controlled amount of aggressive agents (specified in SAE J1681; includes modest additions of water, acetic and sulfuric acids, and sodium chloride) have been added to simulate relatively aggressive – from a potential corrosion perspective – allowable compositions in fuel-grade ethanol.

Results from the initial testing suggest many of the aluminum alloys are relatively immune to corrosion under the test conditions employed. One notable exception was alloy 356, which exhibited extensive corrosion in CE50a (but not in CE85a). Figure 1 shows the autoclave internals immediately following exposure. The specimen supporting a substantial accumulation of corrosion products (at the right-hand end of the specimen rack) is the alloy 356 specimen. Figure 2 shows the specimen rack after removal from the test vessel – the corrosion products (not yet identified) were highly hydrated and substantially gel-like in consistency. Following removal of the corrosion products, the alloy 356 specimen was found to be substantially corroded at/near the crevice washer contact points but relatively uncorroded on the remainder of the specimen. Local wastage of over 0.6 mm (25 mils) was observed (corresponding to a localized corrosion rate of over 3 cm/y). Preliminary metallographic analysis suggests

the aluminum-rich matrix corrodes preferentially compared to Si-rich particles within the matrix. Additional exposures will be performed in the coming quarter, and Fe-based valve seat ring materials will also be incorporated into the testing.

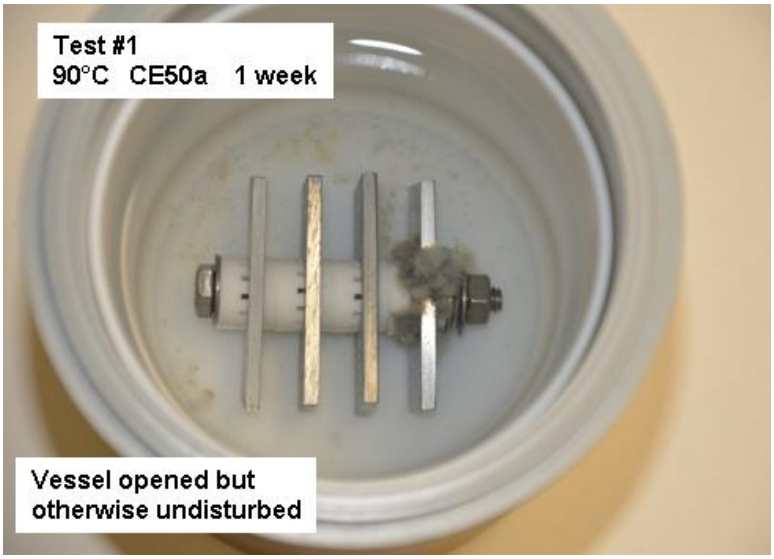

Figure 1. Looking down into the opened autoclave immediately following the test exposure, with test fluid still in place. Teflon crevice washers (slotted) were pressed against one side of each specimen and Teflon shoulder washers were used to isolate the specimens from each other and the stainless steel mounting hardware. Alloy 356 is the right-most specimen in the photograph above, and corrosion product accumulation around the crevice washer is apparent.

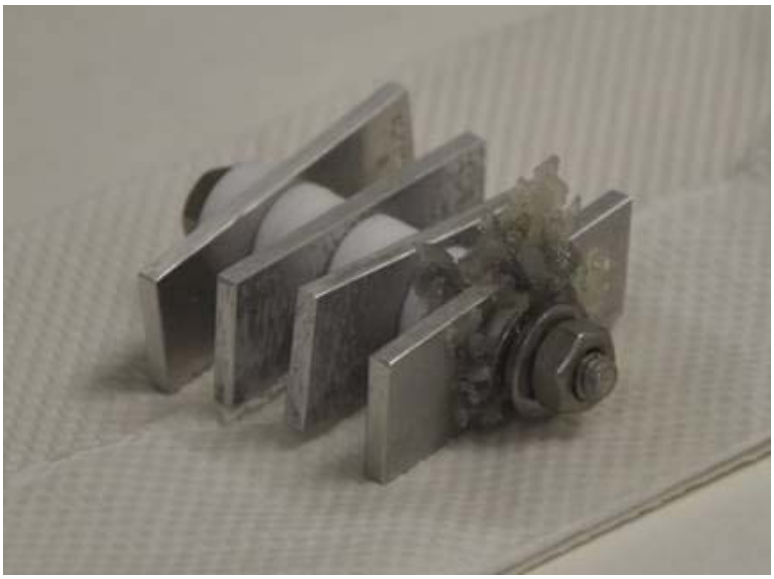

Figure 2. Specimen rack removed from the autoclave following 1-week exposure to CE50a at 90°C. Corrosion product accumulation is restricted to regions at/near the crevice washer on alloy 356 aluminum. The other alloys experienced only very light and irregular discoloration but no measureable corrosion.

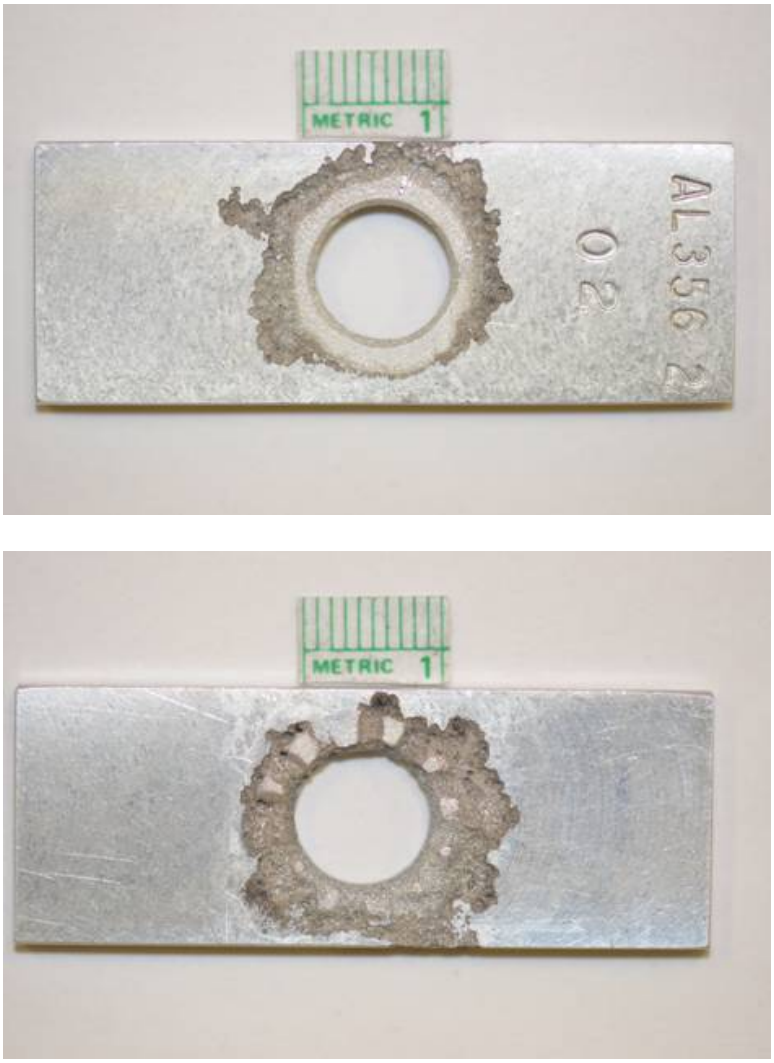

Figure 3. Major test surfaces of the alloy 356 aluminum specimen following exposure for 1 week in CE50a at 90°C. Corrosion products were cleaned from the specimen via ultrasonic cleaning in fresh ethanol followed by a similar treatment in acetone and forced air drying. Metal wastage up to about 0.6 mm (25 mils) was observed in many areas at/near the crevice washer.

Status of FY2011 Milestones

Ongoing.

Communications/Visits/Travel

Routine electronic mail and regular telephone contact (bimonthly conference calls) is being maintained between the USCAR Partners and the ORNL team. No travel occurred this quarter.

Problems Encountered

There has been some difficulty preparing engines for sampling of fluids behind the valve seat crevice (Task 2). In this quarter, machining was finally accomplished on an engine head that resulted in a sampling port intersecting the seat pocket at an appropriate

location and in a manner that does not interfere with engine operation. Assuming follow-on leak testing yields appropriate results, other heads will be similarly machined and engine testing commenced as soon as appropriate facilities are identified.

Publications/Presentations/Awards

none

References

none

Agreement 18571: Materials Issues Associated with Exhaust Gas Recirculation Systems

M. J. Lance, C. S. Sluder and J. M. E. Storey
Oak Ridge National Laboratory

Objective/Scope

Provide information to industry specialists about fouling deposit properties so as to enable improved models and potential design improvements to reduce fouling and its impact on the performance of EGR (exhaust gas recirculation) coolers.

Technical Highlights

In February of 2009, a consortium consisting of engineers responsible for EGR systems was assembled from nine diesel engine manufacturers and surveyed to identify the biggest problems facing EGR systems. EGR cooler fouling was identified as a very critical concern. Each member of the EGR consortium agreed to provide a cooler that had seen enough operation to categorize it as 'half-useful-life'. Of the nine members, the seven companies that currently use HP-EGR all sent at least one fouled cooler for analysis with the results to be shared with the entire consortium.

Neutron tomography is being investigated as a way of non-destructively imaging the deposit on the inside of heat exchangers. Since neutrons transmit through metal and are attenuated by hydrogen, hydrocarbon in the deposit will preferentially block neutrons from transmitting to the detector. Samples are rotated and 720 images are collected and reconstructed to provide a 3-D tomograph of the sample. Figure 1 shows a slice taken from a tomographic set of a cylindrical tube geometry cooler that has a single spiral running down the length of the tube. For this slice, it was determined that the deposit was thinner on top of the turbulator (the flat region of the tube) but thicker on either side. Figure 2 shows a 2 dimensional map of the same sample. Here delaminations between the deposit and the metal wall can be observed. These results show that neutron tomography can be used to observe the location of the deposit with respect to the cooler geometry and to identify potential deposit removal mechanisms.

Status of FY2011 Milestones

Assemble and test sampling system for controlled deposit formation. (10/10) *On Schedule.*

Communications/Visits/Travel

None.

Problems Encountered

None.

Publications/Presentations/Awards

Paper:

- Michael J. Lance, Charles Scott Sluder, John M.E. Storey, and Samuel A. Lewis "Characterization of Field-Aged EGR Cooler Deposits," SAE 2010-01-2091.

Presentations:

- Michael J. Lance, Charles Scott Sluder, John M.E. Storey, and Samuel A. Lewis "Characterization of Field-Aged EGR Cooler Deposits," SAE Fuels & Lubes Meeting 2010.
- Michael J. Lance, Hassina Bilheux, Keely Willis, Andrea Strzelec, C. Scott Sluder, "Characterization of Field-Aged Exhaust Gas Recirculation Cooler Deposits using Neutron Tomography," GPC 2010- Global Powertrain Congress.

Awards:

- 2010 SAE Excellence in Oral Presentation Award
- Work selection for publication in Dec 2010 issue of the SAE International Journal of Engines.

<u>References</u>

None.

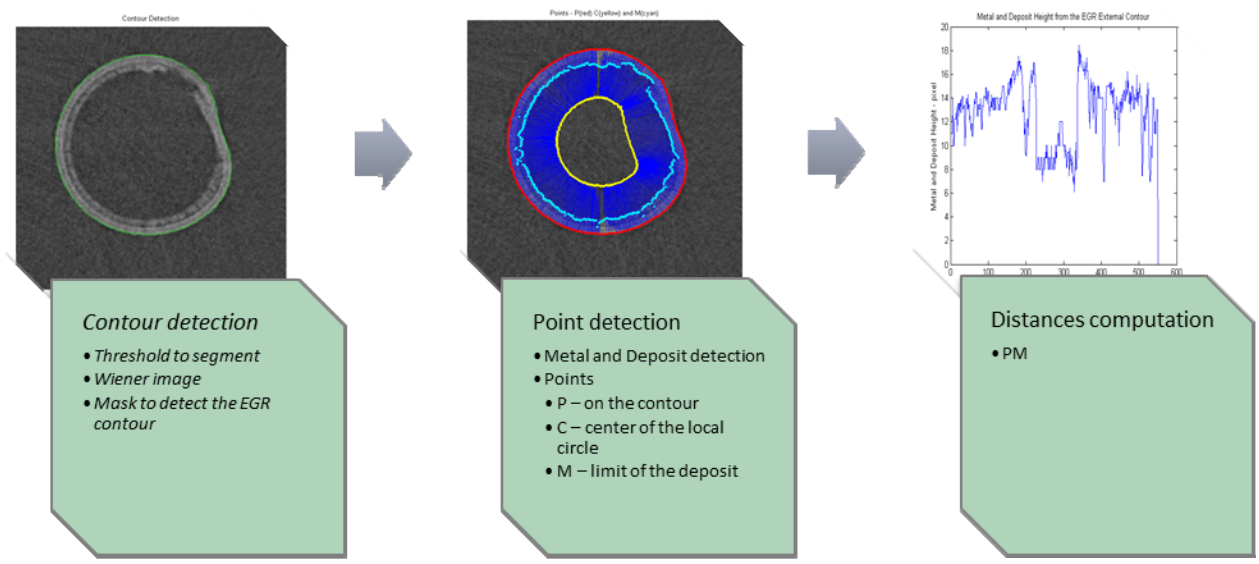

Figure 1. One neutron image generated from a 3-D tomographic set of a tube from cooler #1. The image is processed in order to measure the thickness of the deposit as a function of the radius around the tube.

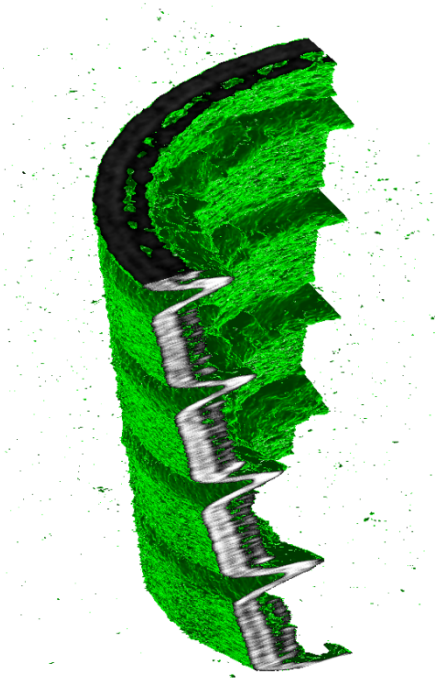

Figure 2. One-quarter isosurface of cooler #1.

Agreement 19202 – Titanium Friction and Wear
(Surface Engineering of Bearing Components)

Peter Blau and Dinesh Bansal
Oak Ridge National Laboratory

Objective/Scope

Energy efficiency and durability of internal combustion engines (ICEs), whether fueled by conventional or alternative fuels, benefits from the utilization of lightweight materials. Examples include fiber composites and alloys of aluminum, magnesium, and titanium. While such materials offer attractive efficiency gains, their use also presents technical and economic challenges. One class of ICE applications involves tribological aspects: that is, those which concern friction, wear, and lubrication. Studies in the United States, Japan, and the United Kingdom have shown that mechanical losses comprise about fifteen percent of the energy dissipation from fuel in a typical ICE, and that of those, energy losses by friction comprise about eighty percent. The two major subsystems, in terms of engine frictional losses, are the piston ring/cylinder interface and the crankshaft bearings, including those on the connecting rods. Past projects at ORNL have focused on the piston ring/cylinder interface. The current project which began in FY 2010 not only addresses the connecting rod bearings, but it also demonstrates surface engineering technologies that could benefit other friction- and wear-critical applications as well.

The objective of this project is to *enable the expanded use of strong, lightweight titanium (Ti) alloys for wear and friction-sensitive engine components like connecting rods (CRs) and crankshafts.* The goal is to evaluate and identify the best available surface engineering methods, whether commercialized or experimental, to reduce friction and wear of Ti alloys under engine-like contact conditions. This work compliments recent developments in Ti processing technology aimed at reducing raw material cost. It utilizes the experience and capabilities of ORNL to effect changes in surface-critical properties via a variety of potential treatment routes. The three phases of this effort are: 1) *Friction and wear baseline screening* of multiple surface treatments and coatings for titanium using ASTM test methods to down-select leading performers for more rigorous year 2 evaluation, 2) *Design and construction of a computer-controlled, variable load bearing tester* (VLBT) to simulate the contact pressure and lubricant regime excursions experienced by connecting rod bearings, and 3) *Development of a prototype diesel engine Ti-based connecting rod concept* using surface-engineered bearing surfaces.

During FY 2010, a series of 21 materials and surface treatments were obtained and evaluated using ASTM G133, a reciprocating friction and wear test method whose development was supported under a previous DOE/OVT project. Pass-fail criteria, based on friction, wear, and vibration were developed and used to down-select leading candidates for more rigorous study in FY 2011 using the VLBT. Results were submitted to, and accepted by, the International Conference on Wear of Materials (April 2011). As described here, an additional study of the best candidates is underway in parallel with the final construction of the VLBT.

Technical Highlights

Detailed studies of down-selected surface treatments continue. Figure 1 summarizes the average coefficients of friction (COF) during reciprocating pin-on-flat sliding experiments in diesel engine oil for all surface treatments evaluated during FY 2010 (for specific testing details see the FY 2010 annual report for this project). In addition to monitoring the experiments for unusual vibrations or abnormally-high wear losses, a failure criterion of COF higher than 0.15 was selected to screen the surface treatments and coatings. The nitrided (NR) and oxygen diffusion (OD) treated specimens yielded the lowest COF among those with diffusion treatments. Among the coatings, titanium-nitride (TiN) and chromium-nitride (CrN) had the lowest COF.

Figure 2 presents the wear volumes of the flat specimens and the AISI 52100 bearing steel ball specimens for the flat surfaces that 'passed.' The DLC and CrN treatments had the lowest total wear of ball and flat specimens, and all four treatments of Ti alloys had more than ten times lower wear than that of the bearing bronze (BB) specimens. For all but one case, the flat specimen exhibited a lower wear volume than that of the ball. The CuNiIn thermal-spray coated bearing bronze had a splat-like microstructure that probably wore unevenly, producing rough-edged features that more strongly abraded the steel ball. During this quarter, a study of the friction and wear behavior of down-selected surface treatments was undertaken in order to better understand the fundamental reasons for their different responses to sliding contact.

Scanning electron microscopy (SEM) of cross-sections of the wear tracks on the flat specimens is being conducted to study the failure modes of selected surface treatments. For example, Figures 3(a) and 3(b) present the end-on views of wear tracks for CrN-coated and OD-treated specimens. In both cases, the wear surface is located at the bottom of the image. The plastic deformation of the substrate material (Ti-6Al-4V) and the manner in which the hard coating (CrN) complies to and protects the undulating shape of the plastically deformed substrate can be clearly seen in Fig. 3(a). Brittle-appearing surface features and pits are evident in Fig. 3(b), but some of the apparent damage in the wear track may have occurred during cross-sectioning. The OD zone is as much as five times harder than the substrate below it, imparting better wear resistance but at the same time reducing ductility. The irregularly-shaped, light-shaded particles shown in Fig. 3 (b) will be analyzed to determine their compositions.

Progress of Construction of the Variable Load Bearing Test System (VLBT). Construction of the VLBT continued this period. Specifically, a new computer for controlling the motor speed and force actuators, as well as providing data acquisition was installed. A heavy machine table and a solid base plate with pre-drilled holes were purchased and fastened together to support the entire system. A 3-phase power supply for the variable-speed drive motor was wall-mounted and connected by electricians. The shaft drive motor along with its controller, bearings, alignment couplings, torque transducer, and rotating specimen holders were assembled. The stationary specimen holder and lubricant supply hardware are still to be fabricated and installed. Orders for load cells to measure normal and tangential forces, signal conditioners, and a data acquisition board for the computer were delayed until new funding arrived, but these remaining parts are expected to be ordered during January 2011.

Future Plans. Plans for the upcoming quarter include: (1) ordering and installing the remaining VLBT parts, completing its construction, and calibrating the machine, (2) conducting bench-mark tests on non-treated titanium and bearing bronze, and (3) continuing studies of the mechanisms responsible for improved friction and wear performance of the down-selected candidate surface treatments and coatings.

Status of FY 2010-11 Milestones

Design friction and wear testing apparatus to simulate connecting rod motions, loads, and speeds, and complete a series of baseline experiments on small test coupons of candidate titanium alloys, with and without surface treatments. **(09/10)** *Status: design completed***.**

Complete construction of a variable-load bearing test system and conduct baseline experiments to establish its operating characteristics. **(03/11)** *Status: in progress.*

Complete tests of candidate coatings and multiple surface treatments using the variable-load bearing test system**. (09/11)** *Status: to begin in Quarter 3.*

Communications/Visits/Travel

Discussions were held with Cummins Engine Company concerning the design of connecting rods in heavy duty diesel engines.

Problems Encountered

A delay in completing the variable-load bearing test system was encountered due to unavoidable changes in funding allocations, but progress is now on track for a mid-Spring completion of apparatus construction, and the milestones for FY 2011 are expected to be completed on schedule.

Reference

1. J. Qu, P. J. Blau, J. Y. Howe, and H. M. Meyer III (2009) “Oxygen diffusion enables anti-wear boundary film formation on titanium surfaces in zinc-dialkyl-dithiophosphate (ZDDP)-containing lubricants,” *Scripta. Metall*., 60, pp. 886-889.

Publications/Presentations/Awards

1) D. Bansal and P. Blau, “Surface engineering to improve the durability and lubricity of Ti-6Al-4V alloy,” accepted for presentation at the 2011 International Conference on Wear of Materials (April 3-7, 2011, Philadelphia), and for publication in the journal *Wear*.

2) A second manuscript, titled: “Wear performance evaluation of oxygen diffusion treated Ti-6Al-4V alloy,” is in preparation and planned for submission to the *Journal of Materials Science and Engineering: A*.

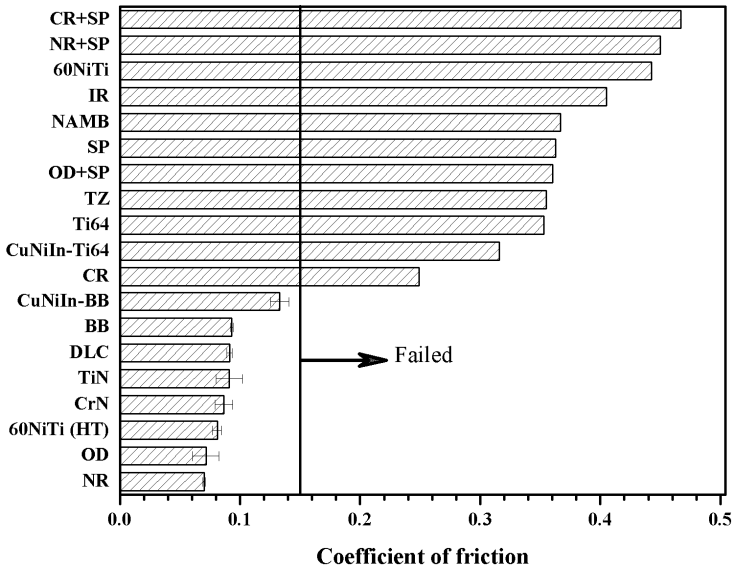

Figure 1. Friction coefficients for 52100 steel balls against various flat specimens (ASTM G133, modified procedure B).

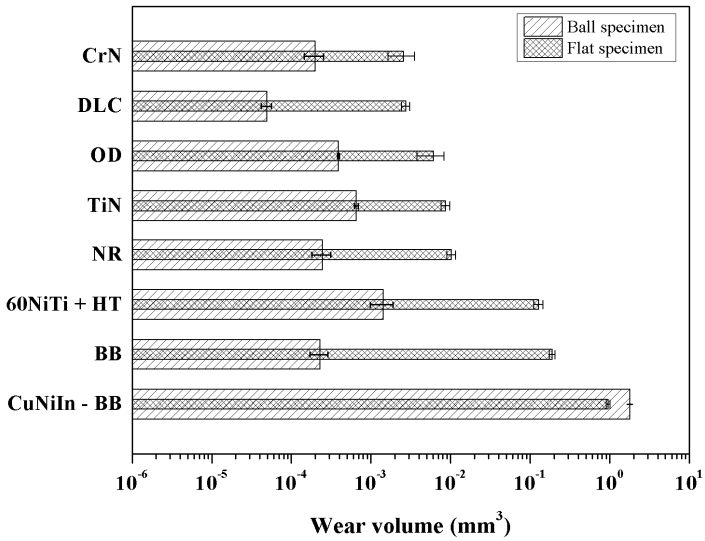

Figure 2. Wear volumes for 52100 steel balls against various flat specimens (ASTM G133, modified procedure B).

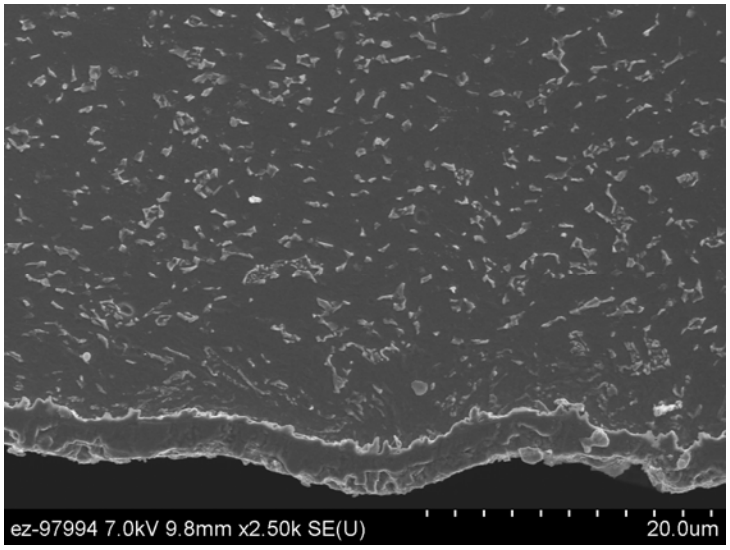

(a)

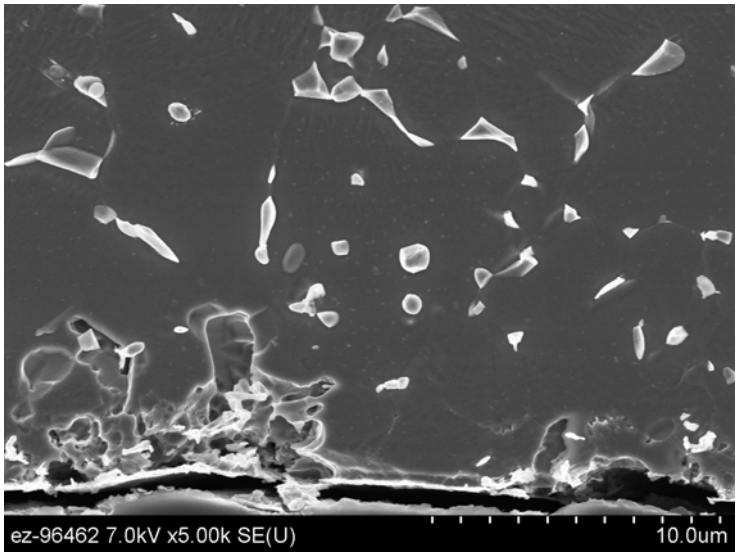

(b)

Figure 3. Scanning electron micrographs of cross-sections of the wear tracks on flat specimens. (a) CrN coating follows the contour of the deformed substrate, (b) embrittlement and pitting of near-surface regions on the OD titanium specimen. Care must be taken to remove the thin scales on the OD titanium after heat treatment, but before testing, to expose the beneficial OD layer. Prior ORNL work showed that the OD layer reacts favorably with oil additives to form anti-wear films [1].

Agreement 10635: Catalysis by First Principles - Can Theoretical Modeling and Experiments Play a Complimentary Role in Catalysis?

C. Narula, M. Moses DeBusk, Xiaofan Yang
Oak Ridge National Laboratory

Objective/Scope

This research focuses on an integrated approach between computational modeling and experimental development, design and testing of new catalyst materials, that we believe will rapidly identify the key physiochemical parameters necessary for improving the catalytic efficiency of these materials. The results will have direct impact on the optimal design, performance, and durability of supported catalysts employed in emission treatment; e.g., lean NO_x catalyst, three-way catalysts, oxidation catalysts, and lean NO_x traps etc.

The typical solid catalyst consists of nano-particles on porous supports. The development of new catalytic materials is still dominated by trial and error methods, even though the experimental and theoretical bases for their characterization have improved dramatically in recent years. Although it has been successful, the empirical development of catalytic materials is time consuming and expensive and brings no guarantees of success. Part of the difficulty is that most catalytic materials are highly non-uniform and complex, and most characterization methods provide only average structural data. Now, with improved capabilities for synthesis of nearly uniform catalysts, which offer the prospects of high selectivity as well as susceptibility to incisive characterization combined with state-of-the science characterization methods, including those that allow imaging of individual catalytic sites, we have compelling opportunity to markedly accelerate the advancement of the science and technology of catalysis.

Computational approaches, on the other hand, have been limited to examining processes and phenomena using models that had been much simplified in comparison to real materials. This limitation was mainly a consequence of limitations in computer hardware and in the development of sophisticated algorithms that are computationally efficient. In particular, experimental catalysis has not benefited from the recent advances in high performance computing that enables more realistic simulations (empirical and first-principles) of large ensemble atoms including the local environment of a catalyst site in heterogeneous catalysis. These types of simulations, when combined with incisive microscopic and spectroscopic characterization of catalysts, can lead to a much deeper understanding of the reaction chemistry that is difficult to decipher from experimental work alone.

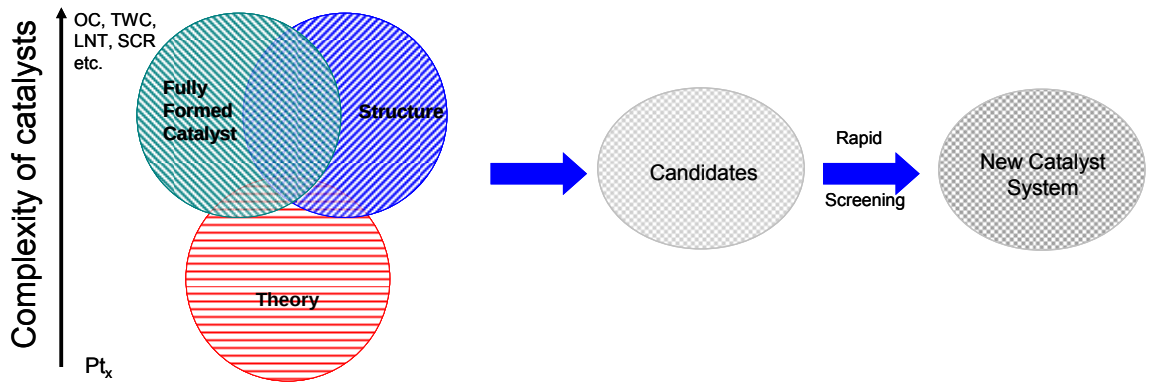

Thus, a protocol to systematically find the optimum catalyst can be developed that combines the power of theory and experiment for atomistic design of catalytically active sites and can translate the fundamental insights gained directly to a complete catalyst system that can be technically deployed.

Although it is beyond doubt computationally challenging, the study of surface, nanometer-sized, metal clusters may be accomplished by merging state-of-the-art, density-functional-based, electronic-structure techniques and molecular-dynamic techniques. These techniques provide accurate energetics, force, and electronic information. Theoretical work must be based on electronic-structure methods, as opposed to more empirical-based techniques, so as to provide realistic energetics and direct electronic information.

A computationally complex system, in principle, will be a model of a simple catalyst that can be synthesized and evaluated in the laboratory. It is important to point out that such a system for experimentalist will be an idealized simple model catalyst system that will probably model a “real-world” catalyst. Thus it is conceivable that “computationally complex but experimentally simple” systems can be examined by both theoretical models and experimental work to forecast improvements in catalyst systems.

We have focused on the oxidation catalyst and SCR catalyst to develop and demonstrate catalyst by design protocol as a prelude to developing catalyst by design protocols for complex emission treatment catalysts; e.g., TWCs, NO_x traps, and HC-SCR catalysts. Our goals are as follows:

- Our theoretical goal is to carry out the calculation and simulation of realistic supported Pt nanoparticle systems (i.e., those equivalent to experiment), in particular by addressing the issues of complex cluster geometries on local bonding effects that determine reactivity. As such, we expect in combination with experiment to identify relevant clusters, and to determine the electronic properties of these clusters. In addition, we plan to study zeolite structures with a view to develop an insight on the mechanistic aspects of catalytic process to enable us to develop better catalysts.
- Our experimental goal is to synthesize metal carbonyl clusters, decarbonylated metal clusters, sub-nanometer metal particles, and metallic particles (~5 nm) on

alumina (commercial high surface area, sol-gel processed, and mesoporous molecular sieve), characterize them employing modern techniques including Aberration Corrected Electron Microscope (ACEM), and evaluate their CO, NO_x, and HC oxidation activity. Furthermore, guided by theoretical studies we plant to synthesize new zeolites and characterize them.

- This approach will allow us to identify the catalyst sites that are responsible for CO, NO_x, and HC abatement. We will then address design of new durable catalysts systems that can withstand the prolonged operations.

Technical Highlights

Until recently, our theoretical studies have focused on supported noble metals. We have shown that single platinum atoms supported on θ-alumina slab contain platinum atom is in the zero oxidation state. This result is very different from that reported in literature on single platinum atoms supported on α-alumina or simplified models of γ-alumina where a platinum atom generally has an unpaired electron. This also means that mechanism of CO, NO_x, or HC oxidation on Pt(0) will be different from that on Pt(I) or Pt(II). We plan to carry out first principle studies of CO oxidation on Pt atoms supported on θ-alumina slab.

Since our experimental work has already shown that the distribution of platinum on γ-alumina and θ-alumina is almost identical, and the surface properties and CO oxidation of both catalysts are identical, we propose that Pt supported on θ-alumina is a better model for Pt supported on γ-alumina than Pt supported on α-alumina or simplified models of γ-alumina.

We have also shown that incorporation of palladium in platinum particles at sub-nanometer scale is quite ineffective in improving the durability, however, large Pt-Pd nanoparticles tend to be more hydrothermally durable than pure Pt particles. While efforts are in progress to prepare sub-nanometer Pt-Pd particles to validate the results of theoretical studies, we have initiated theoretical studies of SCR-zeolite-catalysts.

In this report, we describe our results on theoretical models of Cu-ZSM5 structures. First we optimized all silica ZSM-5 with 96 silicon atoms and 192 oxygen atoms in the idealized orthorhombic unit cell with space group Pnma and unit cell parameters of a=20.1, b=19.9, and c=13.4Å. Our optimized unit cell parameters are a=20.089, b=19.7379, and c=13.141Å which compare well with the experimental values. From this optimized structure, we derived twelve Cu-ZSM-5 structures with two aluminum atoms and one copper atom as a cation to balance the negative charge introduced by replacing silicon with aluminum [Figure 1

A square planar geometry of Cu^{2+} has been deduced from EXAFS studies of Cu-ZSM-5. Since Cu-ZSM-5 is a highly efficient heterogeneous catalyst and reactive gases follow the path of least resistance, we selected possible Cu^{2+} locations on the inner shell of the two major channels in the ZSM-5 structure that can provide maximum contact between the zeolite and reactant gases - straight channel along the y axis and zigzag channel along z axis identified in the ZSM-5 crystal structure.

Figure 1highlights the repeating units from both straight and zigzag channels in green and blue, respectively. Five possible Cu^{2+} binding sites are specified in Figure 1 on the straight channels and another eight Cu^{2+} binding configurations in the zigzag channels. In general, the coordination of a single Cu^{2+} with a square planar geometry involves binding to four oxygen atoms that belong to two negatively charged $[AlO_3]^-$ supporting unit.

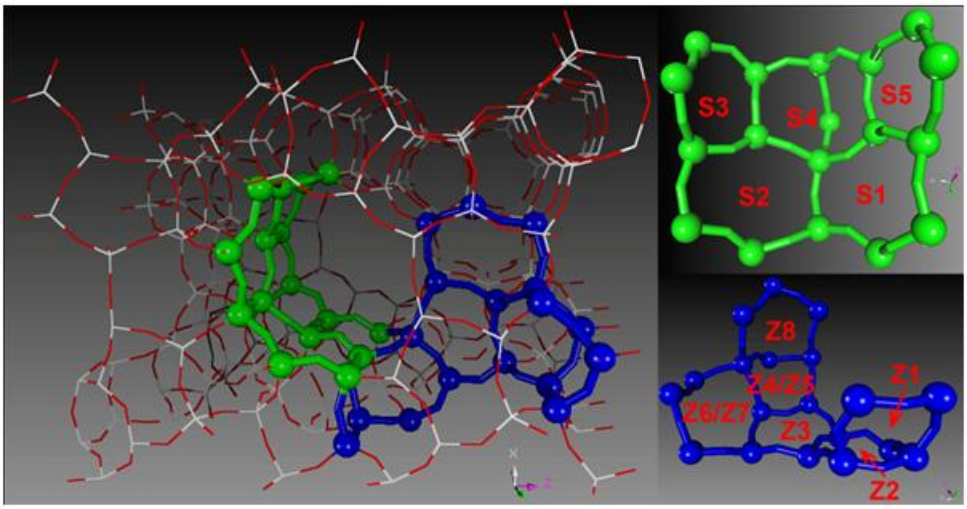

Figure 1: ZSM-5 Structure

The copper binding locations categorized as follows:

- Within a six member ring (neglecting the oxygen atoms), e.g., S1, S2, S4, Z8, and Z6/Z7;
- Within a five member ring, e.g., S3, S5, Z2, Z3, and Z4/Z5;
- Within a four member ring, e.g., Z1.

The optimized structures from quantum mechanical simulations on the full zeolite structures and their total energy are shown in figure 2.

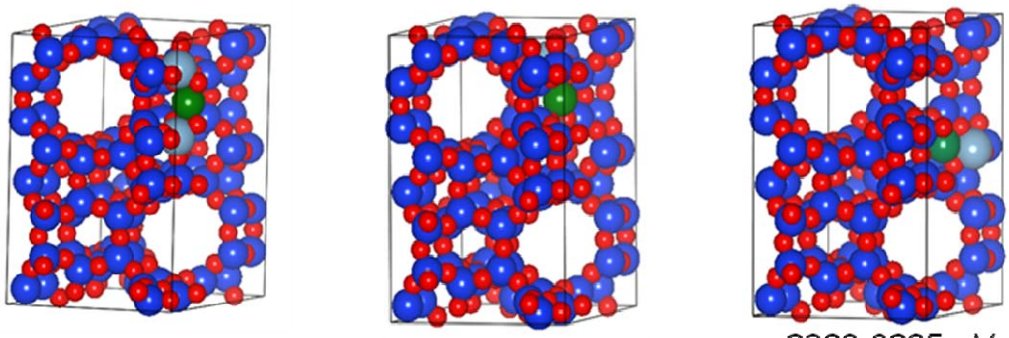

-2326.0142 eV
Cu-ZSM5 L1

-2326.2133 eV
Cu-ZSM5 L2

-2323.8205 eV
Cu-ZSM5 L3

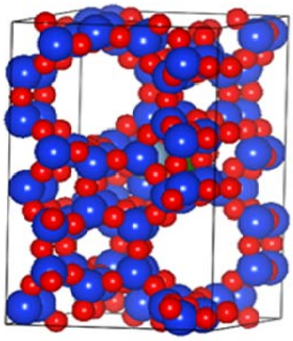

-2323.8856 eV
Cu-ZSM5_4B

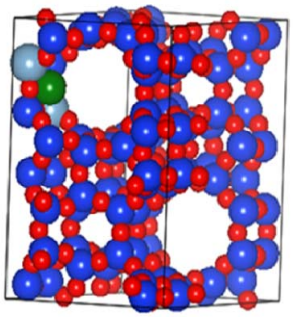

-2324.1694 eV
Cu-ZSM5_Z1

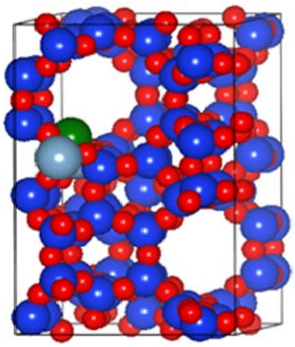

-2325.3333 eV
Cu-ZSM5_Z2A

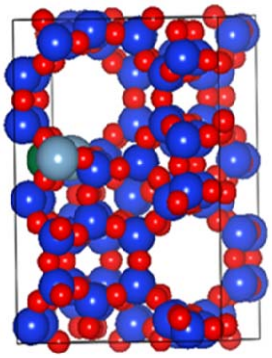

-2324.9811 eV
Cu-ZSM5_Z2C

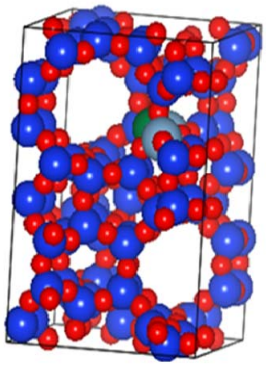

-2325.2546 eV
Cu-ZSM5_Z5

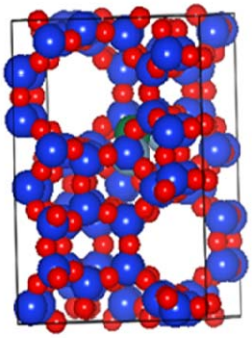

-2325.8502 eV
Cu-ZSM5_Z6

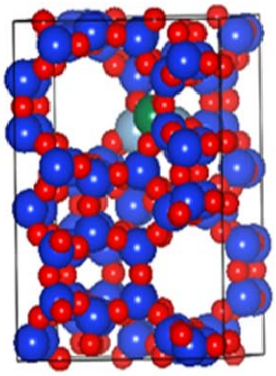

-2325.1622 eV
Cu-ZSM5_Z7

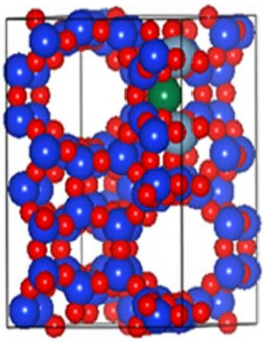

-2325.0515 eV
Cu-ZSM5_Z8

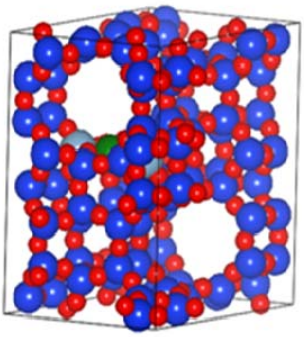

-2325.3359 eV
Cu-ZSM5_Z3A

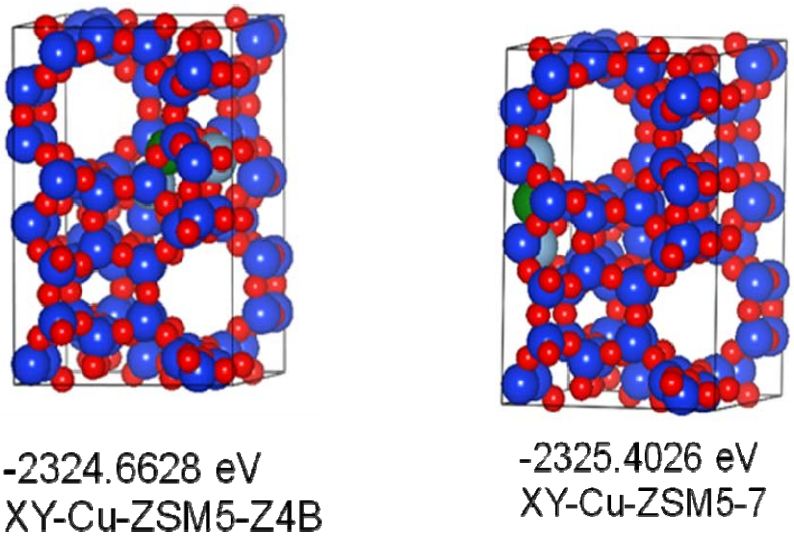

Figure 2: Optimized Cu-ZSM-5 structures and their total energy

In literature, Cu-ZSM-5L1 type models of Cu-ZSM-5 have been proposed to be lowest energy structure. We have found that Cu-ZSM-5L2 structure is also a low-energy structure. The analysis of these structures is in progress and will be reported in the next quarterly report.

Other Activities

A joint project on lean NO_x treatment is on going with John Deere Co under work for others arrangement.

Communication/Visitors/Travel

We have submitted an article titled "Zero oxidation state platinum atom supported on θ-alumina" to Physical Review Letters.

PI is lead organizer of a symposium on emission treatment for energy production and utilization at ACS meeting, Denver, August, 2011

Publications

1. C.K. Narula, X. Chen, M.G. Stocks, Zero oxidation state platinum atom supported on θ-alumina, Physical Review Letters, (submitted)
2. C.K. Narula, "Catalyst by Design – Bridging the Gap between Theory and Experiments at Nanoscale Level" Encyclopedia of Nanoscience and Nanotechnology, Vol. II, Taylor & Francis, New York, 2008, pp 771-782 (invited).
3. C.K. Narula, L.F. Allard, D.A. Blom, M. Moses-DeBusk, "Bridging the Gap between Theory and Experiments – Nano-structural Changes in Supported Catalysts under

Operating Conditions" SAE-2008-01-0416, SAE Int. J. Mater. Manu., 1(2008) 182-188.

4. C.K. Narula, L.F. Allard, D.A. Blom, M.J. Moses, W. Shelton, W. Schneider, Y. Xu, "Catalysis by Design - Theoretical and Experimental Studies of Model Catalysts", SAE-2007-01-1018 (invited).
5. C.K. Narula, M.J. Moses, L.F. Allard, "Analysis of Microstructural Changes in Lean NO_x Trap Material Isolates Parameters Responsible for Activity Deterioration" SAE 2006-01-3420.
6. Y. Xu, W.A. Shelton, and W.F. Schneider, "The thermodynamic equilibrium compositions, structures, and reaction energies of Pt*x*O*y* (*x* = 1-3) clusters predicted from first principles," *Journal of Physical Chemistry B,* 110 (2006) 16591.
7. Y. Xu, W. A. Shelton, and W. F. Schneider, "Effect of particle size on the oxidizability of platinum clusters," *Journal of Physical Chemistry A*, 110 (2006) 5839.
8. C.K. Narula, S. Daw, J. Hoard, T. Hammer, "Materials Issues Related to Catalysts for Treatment of Diesel Exhaust," *Int. J. Amer. Ceram. Tech*., 2 (2005) 452 (invited).

Presentations (last 12 months)

1. Narula, C.K.; Chen, X.; Stocks, G.M., DeBusk, M.M.; Allard, L.F.; "First-Principles and Experimental Studies of the Sub-Nanomenter Platinum Atoms Supported on θ-Alumina" 230th American Chemical Society Meeting, Boston, MA, August 22-26, 2010
2. Narula, C.K.; Chen. X.; Stocks, M.G.; "First-Principles Studies of the Structure and Bonding of Metal Atoms Supported on θ-Alumina," 229th American Chemical Society Meeting, San Francisco, CA, March 21-25, 2010.
3. Moses-DeBusk, M.; Narula, C.K. "Catalyst by design: Combining the power of theory, experiments, and nanostructural characterization for catalyst development," 227th National American Chemical Society Meeting, March 2009 (invited).

Agreement 19214: Effects of Biodiesel Fuel on Diesel Particulate Filter Materials

M. J. Lance, T. J. Toops, S. A. Lewis, J.M.E. Storey and R. M. Connaster
Oak Ridge National Laboratory

Objective/Scope

To characterize changes in the microstructure and material properties of commercial diesel particulate filters (DPFs) in exhaust gas produced by biodiesel blends.

Technical Highlights

Since the degradation of the DPF bricks observed in the first set of samples appeared to be localized in the skin and not the interior, electron probe microanalysis (EPMA) was used to compare the two regions. Figure 1 shows that the interior (channels) appear more porous than the skin which is required for the filter to allow gas to permeate through the walls of the channels but not out of the brick into the padding. The skin also has a broader particle size distribution than the interior presumably to increase its packing density. The skin appears to have at least two phases present; a dense cordierite phase and a glassy grain boundary phase. A fiber phase was also observed in the skin. The glassy grain boundary phase appears to be rich in Si and low in Mg and Al compared to the cordierite grains.

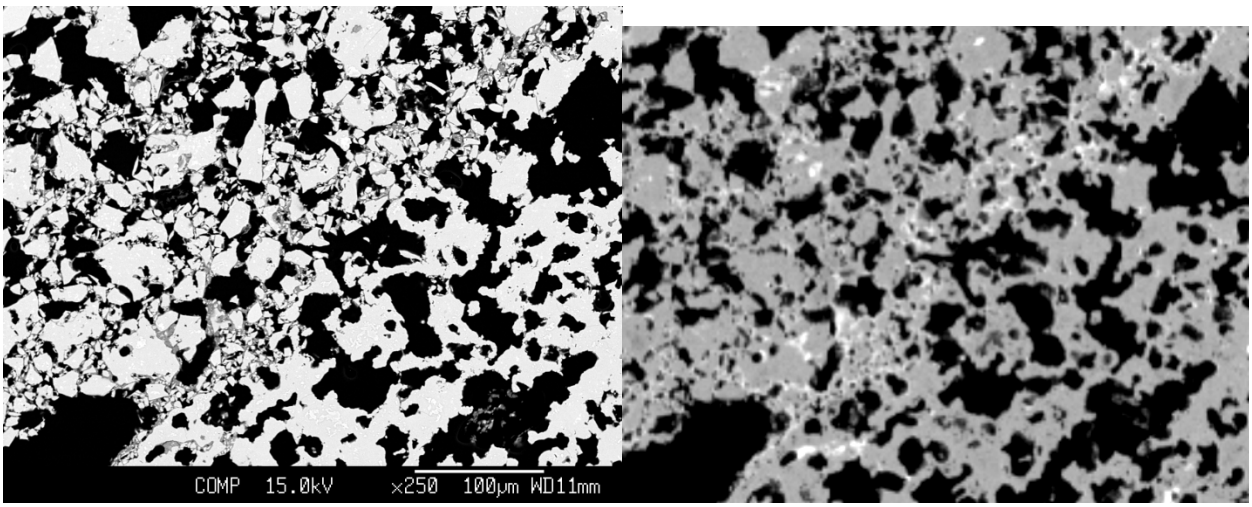

Figure 1. Microstructural Comparison of DPF Outer Skin to DPF Interior. SEM image (left) and an electron probe microanalysis (EPMA) map of silicon (right) show the difference in the interior walls (lower right) and the outer skin (upper left).

In order to reproduce the initial filter degradation, four DPFs were loaded with soot using the same Mercedes engine that produced initial degradation. The engine was operated at 1500 rpm and 2.6 bar. The initial degradation occurred with Soy Gold but this test used SME fuel from Renewable Energy Group (REG) which was certified by Southwest Research Institute (SWRI) and GC-MS at Oak Ridge. Figure 2 shows the surface of the DPF after being exposed to certified B100 exhaust and storage for 3 months. The sample showed no degradation.

Figure 2. Cordierite DPF that had been aged for 3 months after being run with B100 fuel in order to replicate original degradation experiment.

Status of FY2010 Milestones

Measure the chemical composition and pH of condensate and PM generated by a diesel engine running with ULSD and biofuel blends. (12/10) *On Schedule.*

Communications/Visits/Travel

None.

Problems Encountered

None.

Publications/Presentations/Awards

None.

References

None.

Agreement 20091: Electrically Assisted DPF Material

M. J. Lance, A. A. Wereszczak, J. E. Parks, and W. P. Partridge
Oak Ridge National Laboratory

Objective/Scope

In this CRADA project with General Motors (GM), two research objectives are being pursued:

1. Measure of substrate temperatures during DPF regeneration with optically based techniques that are not susceptible to conductive interferences that are problematic for common thermocouple technologies.
2. Analysis of diesel particulate filter (DPF) substrate materials to understand crack and failure mechanisms and resolve current differences in simulation and experimental results.

Technical Highlights

Engine-based DPF Studies

The GM electrically assisted DPF (EADPF) assembly that arrived in FY2010 and was installed on a GM 1.9-liter diesel engine at ORNL was exercised under various operating conditions to determine the correct operating parameters to attain the temperatures necessary for DPF regeneration. Most of the work in this quarter was performed with the EADPF placed downstream of a conventional DPF so that particulate matter (PM) on the EADPF was not an issue in the studies. Engine speed and load combinations were combined with “post” fuel injection (adding additional fuel in-cylinder after the main combustion event) to increase exhaust system temperatures via oxidation of hydrocarbons over the diesel oxidation catalyst. Electric-generated heat was added to different base exhaust temperatures. The experiments conducted served to test the control and power system for the electric heat and understand the engine and EADPF system operation as a whole. Figure 1 shows and example DPF heating event that combines heating via post fuel injection with electrical heating of each of the four heater zones.

In general, the EADPF system and control electronics are working well. However, there are some issues with the thermocouples on the heater element that are causing problems with the controls at the high temperatures required for EADPF operation. The thermocouple signals are dropping out at the high temperatures. The effects were filtered for the data shown in Figure 11, but the problem is significant especially at high temperatures. Next quarter efforts on the project will focus on addressing this issue.

In parallel to the engine dynamometer-based studies on the EADPF system, work is being done to develop a fiber optic-based temperature measurement system that would avoid the conductive biases associated with temperature measurement by thermocouples. Ultimately, the DPF substrate temperature will be measured with the fiber optic technique on the engine-dynamometer system. Progress is being made on bench scale systems to measure blackbody radiation and calibrate the collected light signal against actual temperatures. Figure 2 shows blackbody radiation spectra from a

fiber optic positioned inside a ceramic monolith at three different temperatures. Calibration and data acquisition programming will continue on this effort to enable the technique to be deployed effectively on the engine-based EADPF system.

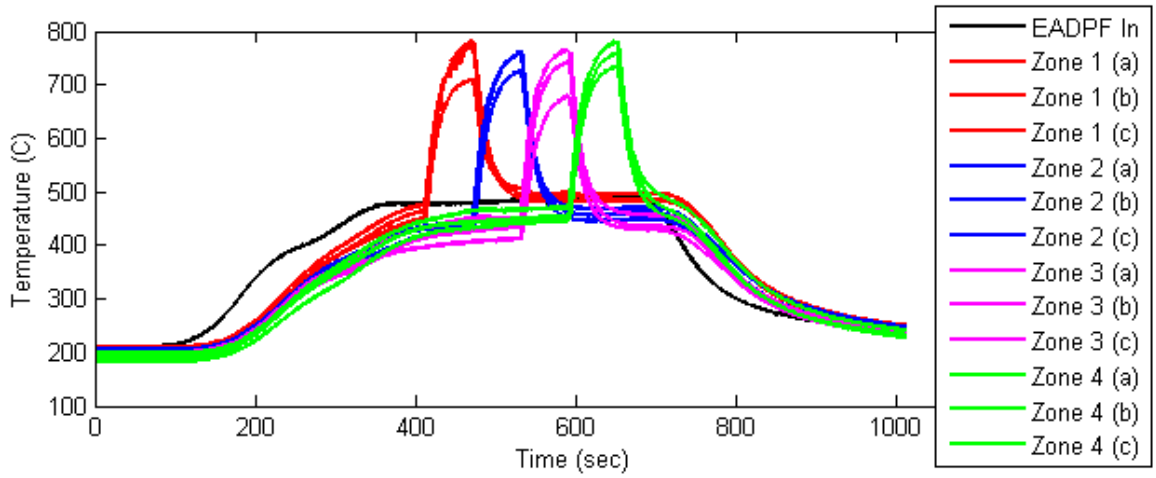

Figure 1. Temperatures recorded during an EADPF heating event. At time=100 sec, post injection fueling was added to raise the exhaust temperature to ~480ºC. At time=400 sec, each of four heater zones were subsequently electrically heated with a fixed 90% duty cycle. The data has been filtered to remove thermocouple signal noise from the heater power cycle.

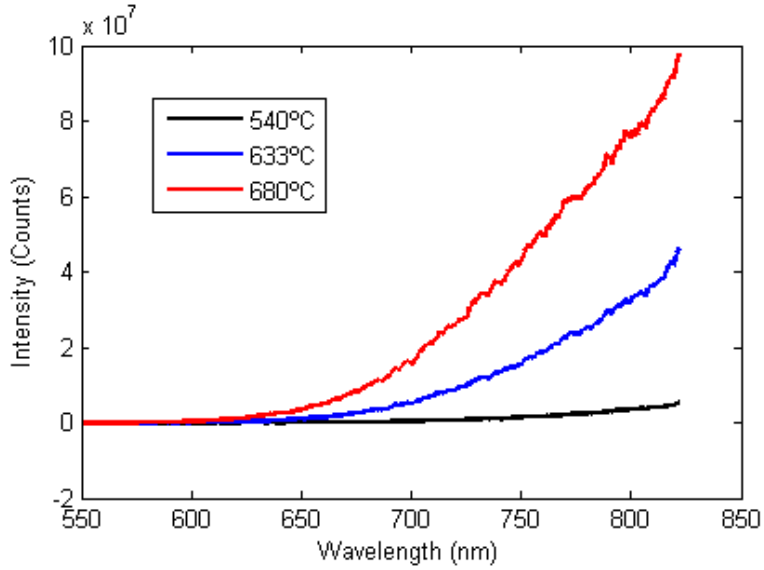

Figure 2. Temperatures recorded during an EADPF heating event. At time=100 sec, post injection fueling was added to raise the exhaust temperature to ~480ºC. At time=400 sec, each of four heater zones were subsequently electrically heated with a fixed 90% duty cycle. The data has been filtered to remove thermocouple signal noise from the heater power cycle.

DPF Mechanical Evaluation

The mechanical testing and finite element analysis continued of specimens for the estimation of (tensile) failure stress as a function of tensile-stress-direction and location. The considered specimens are shown in Fig. 3. Biaxial flexure testing of disks will subject the tensile side of the specimen to an equibiaxial radial tensile stress. Such testing is featured in ASTM C1499 [1]. Such testing is underway on disks machined from the two ends of a DPF and from the DPF interior. Vertically oriented diametral compressive loading of an o-ring specimen geometry will subject the outer diameter to hoop tension at the 3 and 9 o'clock positions and subject the inner diameter to hoop tension at the 6 and 12 o'clock positions. The weakest of those four locations will cause failure and its failure stress will be noted. This test method was developed a while ago to measure failure stress in ceramic tubes [2-3]. Lastly, testing the sectored flexure specimen [4] in 4-pt flexure will subject the exterior of the DPF to an axial tensile stress. The theta specimen, though initially considered, has been dismissed in favor of the more simpler biaxial flexure testing.

O-ring testing was primarily featured during the present quarter, and a seemingly important observation was established that the elastic modulus of the DPF's cordierite is much lower than thought. Our estimation of failure stress (with all specimens shown in Fig. 3) occurs via the flowchart shown in Fig. 4. Mechanical testing and finite element analysis (FEA) are combined to achieve this. For example, the diametral compression of the o-ring specimen (shown in Fig. 4) produces a definitive relationship between compressive force and load-point-displacement. The same loading scenario is then modeled with FEA (enabled thru ORNL's μ-FEA software and the actual capturing of the DPF strut structure) by adjusting the cordierite's elastic modulus until the experimentally measured load-point-displacement jives with the measured maximum compressive force. When they are correlated, we so far estimate (of several o-ring specimens) an elastic modulus that has a range of 1-2 GPa. This is approximately one order of magnitude lower than reported elastic modulus estimated with sonic- or ultrasonically-based. If our values are indeed correct, then the actual stresses in a DPF during service would be lower than those predicted using the sonic-based elastic modulus values. For example, if we use an elastic modulus of 1-2 GPa for the cordierite, then we estimate a (hoop) tensile failure stress of a couple MPa.

Additional testing of the o-ring, and testings of the biaxial and sectored flexure specimens is continuing in Q2, and further scrutiny of this lowe elastic modulus value will occur.

Status of FY 2011 Milestones

1. Measurement of the fuel penalty for both Electrically-Heated DPF and conventional fuel-heated approaches (September 2011). On Schedule
2. Optimization of the fiber-optic temperature measurement technique and a rigged DPF system with fiber-optic and thermocouple probes ready for engine use (September 2011) Delayed- Thermocouple signals are not behaving as expected in the high temperature region. We are in communication with GM to address this problem.

3. Database of strength-size-scaling statistics of ceramic used in EHDPF (September 2011) On Schedule.
4. Rank properties and geometrical parameters that most affect tensile stresses in EHDPFs (September 2011) On Schedule.
5. Rules of design for EHDPF regenerators (September 2011) On Schedule.
6. Recommendations for the best commercial alloy for this application (September 2011) On Schedule.

Communications/Visits/Travel

1. A CRADA review conference call between GM and ORNL occurred on 08Dec2010.

Problems Encountered

None.

Publications/Presentations/Awards

None.

References

[1] "Standard Test Method for Monotonic Equibiaxial Flexural Strength of Advanced Ceramics at Ambient Temperature," ASTM C1499, Vol. 15.01, ASTM International, West Conshohocken, PA, 2009.

[2] O. M. Jadaan, D. L. Shelleman, J. C. Conway, Jr., J. J. Mecholsky, Jr., and R. E. Tressler, "Prediction of the Strength of Ceramic Tubular Components: Part I - Analysis," *Journal of Testing and Evaluation*, 19:181-191 (1991).

[3] D. L. Shelleman, O. M. Jadaan, J. C. Conway, Jr., and J. J. Mecholsky, Jr., "Prediction of the Strength of Ceramic Tubular Components: Part II - Experimental Verification," *Journal of Testing and Evaluation*, 19:192-200 (1991).

[4] A. A. Wereszczak, S. F. Duffy, E. H. Baker, J. J. Swab, and G. J. Champoux, "Strength of a Ceramic Sectored Flexural Test Specimen," *Journal of Testing and Evaluation*, 36:17-23 (2008).

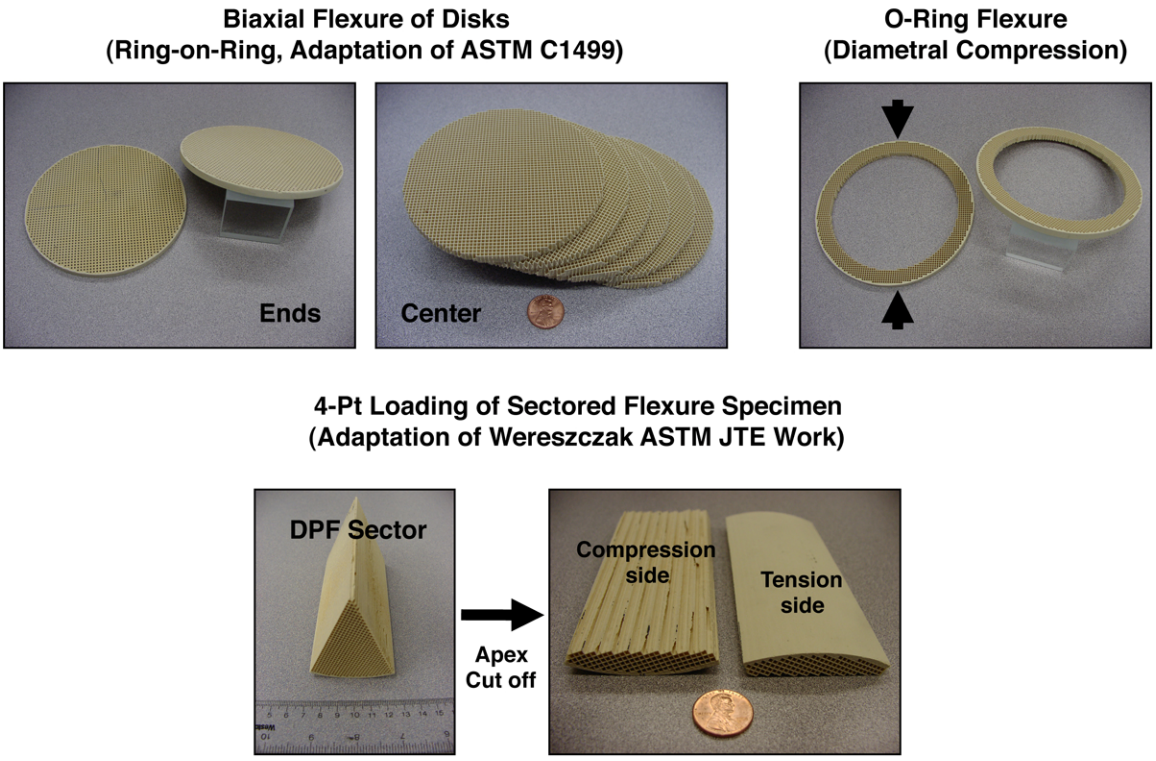

Figure 3. Three different specimen geometries are being mechanically tested to estimate failure stress as a function of direction and location of tensile-stressing.

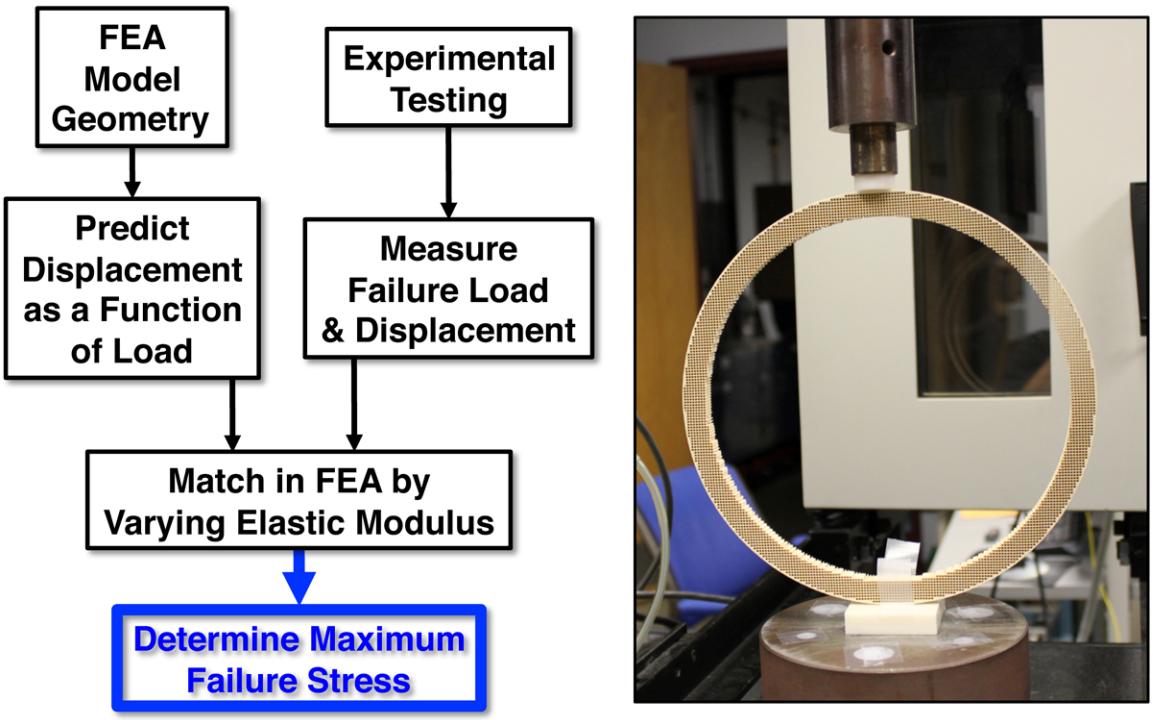

Figure 4. Flowchart (left) describing the modeling and experimentation pathway to determine maximum failure stress, and (right) example of an o-ring test specimen in a mechanical test frame.

Agreement 9105: Ultra-High Resolution Electron Microscopy for Characterization of Catalyst Microstructures and Reaction Behavior

L. F. Allard, C. K. Narula, W. C. Bigelow, D. P. Nackashi, J. Damiano, and F. H. Ribiero
Oak Ridge National Laboratory

Objective/Scope

The objective of the research is to understand fundamental processes in catalytic systems with applications to transportation technologies, such as those used for the treatment of NO_x emissions, and for the production of biomass-derived liquid fuels. The research heavily utilizes new capabilities and techniques for ultra-high resolution transmission electron microscopy with the HTML's aberration-corrected electron microscope (ACEM). The research is ultimately focused on understanding the effects of reaction conditions on the changes in morphology of heavy metal species on "real" catalyst support materials (e.g. oxides and carbon materials), and the understanding of the structures of model mono-, bi- and multi-metallic catalyst systems of known particle composition. A major thrust of these studies has been to develop methods of *in situ* microscopy at elevated temperatures and under controlled gas compositions. This work has expanded with the collaboration with Protochips Inc. (Raleigh, NC), who provide a novel heating technology utilizing MEMS-based heating devices that we have shown to be stable enough to provide sub-Ångström imaging capabilities at high temperature in the ACEM. Model samples of nanoparticulates of controlled composition on carbon or oxide supports are also being studied in collaboration with the catalysis group at the University of Texas-Austin (Prof. P. Ferreira), the University of Texas-San Antonio (Prof. M. Jose-Yacaman), the University of Missouri-St. Louis (Prof. J. Liu), and University of New Mexico (Prof. A. Datye). Studies of the behavior of platinum group metal (PGM) species on oxide substrates are also being conducted with Drs. S. A. Bradley of UOP Co., and C. H. F. Peden of PNNL, and Prof. F. H. Ribiero at Purdue University. NOx trap catalyst materials BaO/Al_2O_3 are being studied with Dr. Peden and Dr. Ja Hun Kwak at PNNL and Pt-Re/C catalysts on model carbon nanotube materials are being studies with Drs. Y. Wang and L. Zhang, also of PNNL. We have also initiated a new study of "intelligent catalysts" for automotive emission control applications, based on the self-regenerative phenomenon of heavy metal species such as Pd and Rh in Ca- and La-based perovskite crystal structures. This work is being conducted in collaboration with Prof. Xiaoqing Pan of the University of Michigan, and Ford Research Laboratory colleague Dr. Andrew Drews.

Technical Progress

This report highlights work this quarter on the use of ultra-high-resolution imaging of Au and Pt nanoparticles on oxide supports in conjunction with infra-red spectroscopic techniques to determine active sites on the catalytic materials. Also, in further work on development of an environmental cell capability for *in situ* heating and gas reaction studies, tests conducted on using the "Gen 2" E-cell fabricated in conjunction with Protochips Co. has led a significantly improved design of the cell, called the "Gen 3" E-cell. The Gen 3 cell design and fabrication will be described in a future quarterly.

Determination of Active Sites on Catalytic Nanoparticles

Work in collaboration with the Purdue University group of Prof. F. H. Ribiero has involved high-resolution imaging coupled with Fourier transform infra-red (FTIR) and diffuse reflectance infra-red Fourier transform (DRIFT) spectroscopies to elucidate the active sites on Au and Pt nanoparticles on oxide supports such as alumina, titania and silica. Results from the Au nanoparticle studies are highlighted here.

Bulk Au is in general inert, but in nanoparticle form (i.e. in the nanometer range), it has been shown to be an excellent catalyst for a variety of reactions, including CO oxidation and the water-gas-shift reaction (WGS). The active species or sites on Au-based catalysts have been debated in a number of papers, with perimeter sites on nanoparticles,[1] corner sites of low coordination,[2] gold bilayers[3,4] and cationic gold[5] being proposed. The research reported here uses a model, non-porous support material, TiO_2 (rutile, titania), to simplify the system and enhance the imaging of Au nanoparticles[6] in relation to the support. Characterization of the Au/titania materials with both microscopy and infra-red analysis techniques allows differences in turnover rate (TOR) to be correlated to nano-gold vs bulk gold materials, to further understand why nano-gold is catalytically active.

Active sites for catalysis in the WGS reaction for Au catalysts have been suggested to include the contact between Au clusters and the support, because of the well-known support effect,[7,8] but no full study that relates Au particle size to the rate per active Au species has been performed. Au atoms with lower Au-Au coordination generally show higher TORs than bulk Au (111) surfaces or Au atoms with high Au-Au coordination.[2,9] Thus, this system represents an opportunity to explore the important general question of how catalytic sites are defined in cases where coordinative unsaturation can greatly alter catalytic function.

Au deposited on nonporous rutile TiO_2 was prepared to investigate the active sites for Au nanoparticles. Activity of the catalysts was measured using a plug flow reactor apparatus (not described here), and the particle sizes were evaluated using high-angle annular dark-field imaging (HAADF) in the HTML's JEOL 2200FS aberration-corrected electron microscope operated in scanning transmission mode (STEM). This technique shows Au in bright contrast down to the single atom level, in comparison to the rutile support. The results in Fig. 1 show a clear trend that catalysts with smaller average Au particle size have larger rates per mole of Au. The difference in rate between the largest (6.7nm) and smallest (1.2nm) average particle size samples was over two orders of magnitude. The rate per total mole of Au should vary approximately as d^{-1} for the TOR to remain constant with changes in particle size. Rather than a d^{-1} dependence, we found that the rate per total mole of Au varied with particle diameter as $d^{-2.7 + 0.1}$, which means that the rate per surface Au atom varied roughly as $d^{-1.7}$. Thus, all of the atoms on the surface of each particle *cannot* be considered the active sites if it is assumed that each site has a similar rate independent of Au particle size.

STEM imaging experiments were performed on four different Au / rutile catalysts to determine if only sub-nanometer Au clusters were the active site. A rate per mole of Au was calculated from the rate per gram of catalyst and the estimated surface coverage of sub-nanometer clusters, assuming the sub-nanometer clusters were the active sites. Since this rate is larger than the calculated rate of collision of energetic CO molecules on the same clusters, sub-nanometer clusters cannot be the dominant active sites. This finding agrees with other results which show that CO oxidation rate per Au cluster is significantly decreased for Au clusters below a certain size range of approximately 8 atoms or below 0.8 nm in size.[10,11]

The STEM studies indicate that the Au particle morphology was best described by a truncated cubo-octahedron. Figure 2 shows example HAADF images used to obtain this result. A model was then constructed to calculate the rates for each sample, assuming that different sites are active. This model uses particle size distributions determined from the STEM images in conjunction with information regarding the number of sites for clusters of a particular size determined from the truncated cubo-octahedra model shown in Fig. 3. Density functional theory calculations from this model structure suggest that the most important factor that affects the adsorption and reaction properties of Au atoms is their coordination with other Au atoms. The assumption is that the true TOR does not depend on particle size. A rate for each sample was calculated from the following equation: Rate per mole of Au = $[\Sigma\, c_{site}\, s(d)] / [\Sigma\, t(d)]$, where s(d) is the number of atoms for a cluster of diameter d that correspond to the site of interest, t(d) is the total number of atoms for that cluster; the summation was carried out over all the Au clusters identified from the HAADF STEM image of that catalyst. In other words, the full particle size distribution was used for each sample. The constant c_{site} was calculated from a best fit of the model with the experimental rate data over the full range of average particle sizes represented by all the 14 samples studied. The use of the model rutile support was critical for this study because the HAADF STEM images provided a precise measure of the particle size distribution needed for this analysis.

The data are compared to the results of the model in Fig. 4. The rate per mole of Au varies as $d^{-1.71}$ if atoms on the perimeter in contact with the support are the active sites, and as $d^{-2.82}$ if corner atoms are the active sites. The experimental rate is clearly best fit by the corner model (Fig. 5). A corner model has been used to explain the size effect observed for Au catalysts in the oxidative environment of CO oxidation.[2,12] It is surprising that the model can also be used to explain the particle size dependence in the highly reducing atmosphere present during WGS.
Here a “corner” site is a specific type of site that does not change in absolute number with a change in particle diameter, and exhibits a Au-Au coordination number less than 7. It has been argued that Au atoms in contact with the support will be inactive due to increased coordination provided by the support.[13] As shown in Fig. 3, the corner sites that have contact with the support have a Au coordination number of 4, but those without support contact have a Au coordination number of 6. Although there are differences between these two types of sites, it is clear that a lack of coordination of the Au atoms in the clusters provides the dominant sites. The conclusion that corner atoms are dominant sites implies that the rate on each cluster larger than approximately 1nm

in size is the same, and that the total rate of a given sample is proportional only to the number of clusters, but not their size. To create more stable WGS catalysts with higher rates per mole of Au, it is necessary to maintain small average gold particle sizes to maximize the number of clusters for the weight loading of gold used. The presence of the corner atoms with low Au-Au coordination is caused by the geometry of the nanoparticles. Thus, it is possible to explain the high rate per mole of Au of the nanoparticles without invoking explanations involving changes to the electronic nature of the nanoparticles with size. A question of interest for future work is how the corner sites, implicated by the unusual diameter dependence of the rate per mole of gold found in this work, participate in the dual functionality of WGS catalysts that results from the nature of both the metal and the support.

References:

1. T. Fujitani, I. Nakamura, T. Akita, M. Okumura, M. Haruta; *Angew. Chem., Int. Ed.* ***48***, 9515 (2009).
2. T. V. W. Janssens, B. S. Clausen, B. Hvolbaek, H. Falsig, C. H. Christensen, T. Bligaard, J. K. Norskov; *Top. Catal.* **44**,15 (2007).
3. M. Valden, X. Lai, D. W. Goodman; *Science* **281**,1647 (1998).
4. A. A. Herzing, C. J. Kiely, A. F. Carley, P. Landon, G. J. Hutchings; *Science* **321**, 1331 (2008).
5. Q. Fu, H. Saltsburg, M. Flytzani-Stephanopoulos; *Science* **301**, 935 (2003).
6. Datye, A. K.; *J. Catal.* **216**,144 (2003).
7. J. Li, N.Ta, W. Song, E. S. Zhan, W. J. Shen; *Gold Bull.* **42**, 48 (2009).
8. R. Burch; *Phys. Chem. Chem. Phys.* **8**, 5483 (2006).
9. H. Sakurai, A. Ueda, T. Kobayashi, M. Haruta; *Chem. Commun.* 271 (1997).
10. A. Sanchez, S. Abbet, U. Heiz, W. D. Schneider, H. Hakkinen, R. N. Barnett, U. Landman; *J. Phys. Chem. A* **103**, 9573 (1999).
11. V. Aguilar-Guerrero, R. J. Lobo-Lapidus, B. C. Gates; *J. Phys. Chem. C* **113**, 3259 (2009).
12. S. H. Overbury, V. Schwartz, D. R. Mullim, W. F. Yan, S. Dai; *J. Catal.* **241**, 56 (2006).
13. M. Boronat, F. Illas, A. Corma; *J. Phys. Chem. A* **113**, 3750 (2009).

Status of Milestones

On schedule

Communications/Visits/Travel

None this quarter

Publications

1. Metallic Corner Atoms in Gold Clusters Supported on Rutile are the Dominant Active Site during Water-Gas Shift Catalysis; W.D. Williams, M. Shekhar, W.-S. Lee, V. Kispersky, W. N. Delgass, F. H. Ribeiro, S. M. Kim, E. A. Stach, J. T. Miller and L. F. Allard; *J Amer Chem Soc* (2010) 132 (40),14018–14020

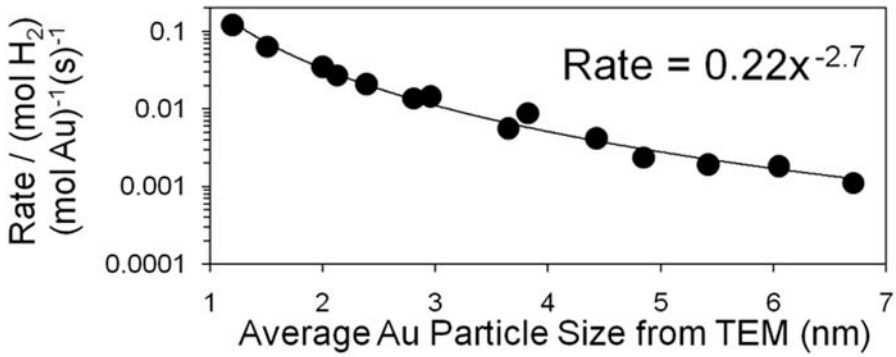

Figure 1. Rate per total mole of Au calculated at 120°C, 6.8% CO, 21.9% H_2O, 8.5% CO_2, and 37.4% H_2 versus average Au particle size.

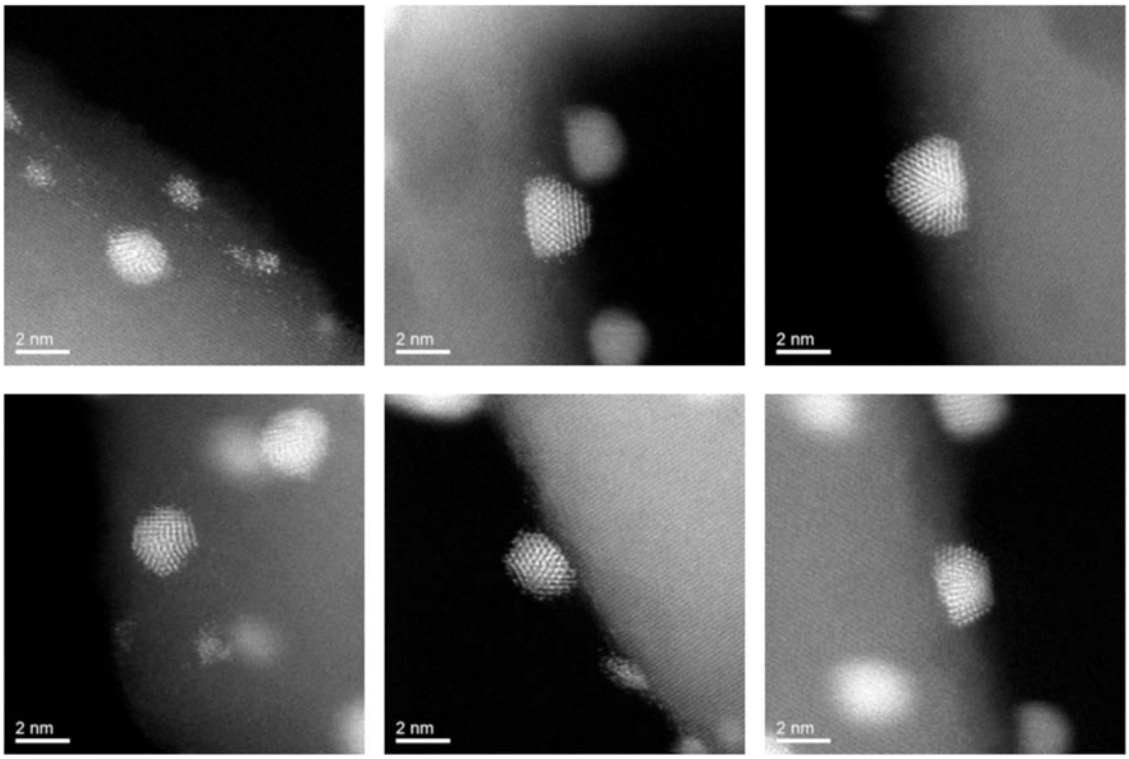

Figure 2. Representative HAADF STEM images of Au atoms and nanoparticles on rutile surfaces, which suggest the cubo-octahedron model of typical Au nanoparticle in this system.

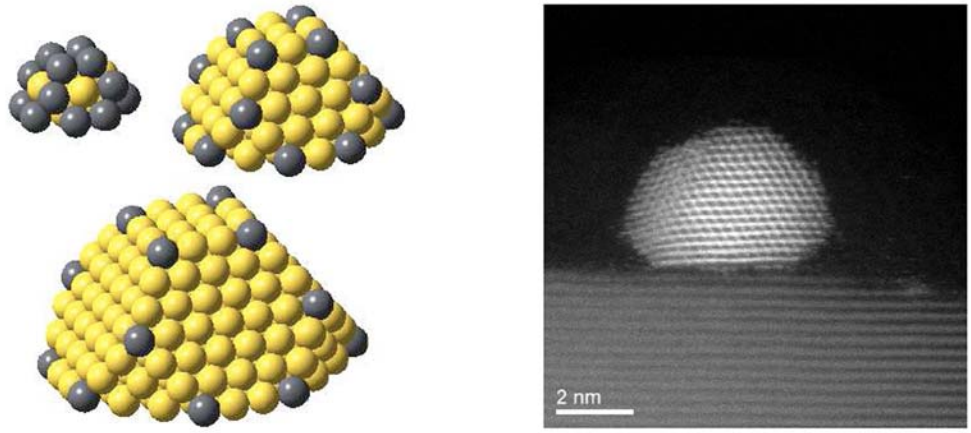

Figure 3. *(Left)* Physical models of corner type sites on truncated cubo-octahedra Au clusters with 25, 119, and 331 atoms based on a *(Right)* typical high angle annular dark field STEM image of a Au nanoparticle.

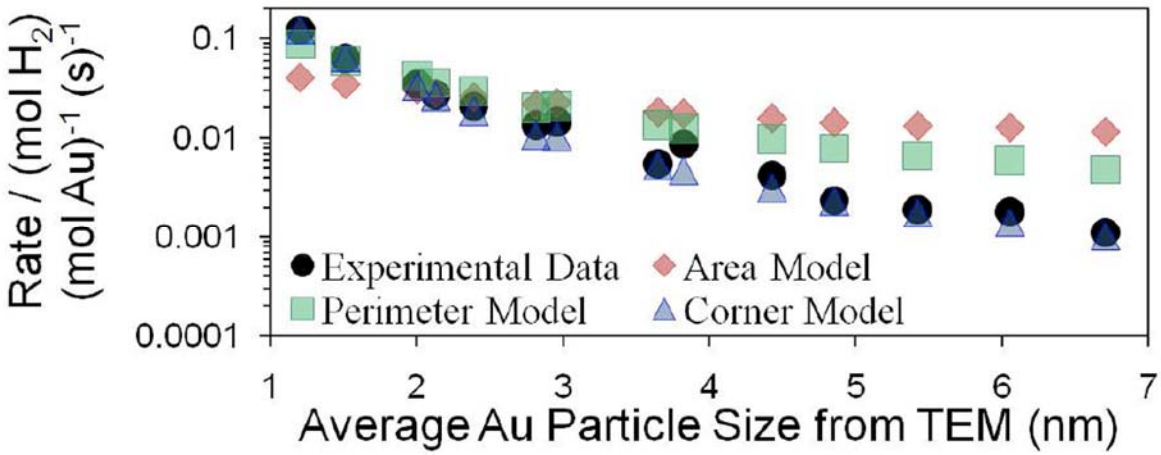

Figure 4. Best fits of model rates to experimental data. The rate per mole of Au varies as $d^{-1.71}$ if atoms on the perimeter in contact with the support are the active sites, and as $d^{-2.82}$ if corner atoms are the active sites.

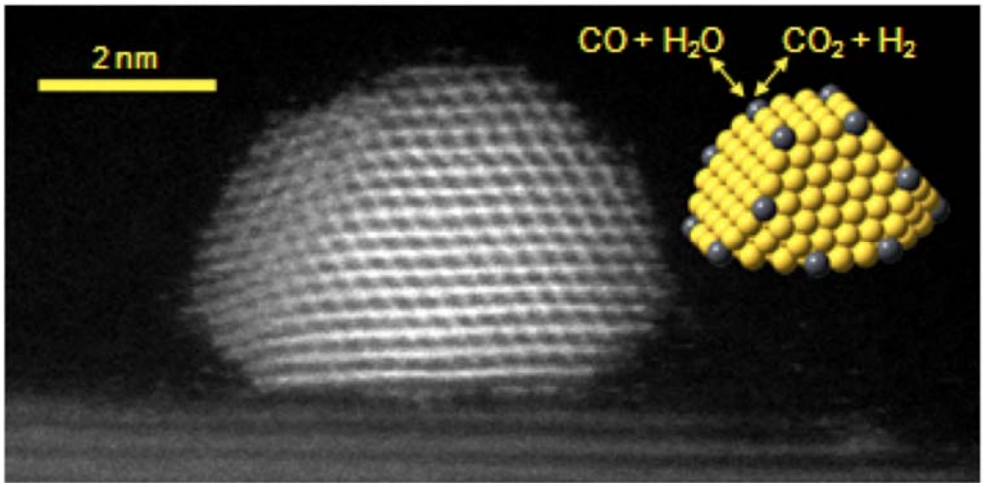

Figure 5. The "corner model" of the Au nanoparticle that best fits the WGS rate data; the reactions at the corner sites are indicated.

Agreement 14957: High Temperature Thermoelectrics

A. A. Wereszczak, H. Wang, R. McCarty
Oak Ridge National Laboratory
and
J. Sharp
Marlow Industries, Inc.

Objective/Scope

Two-thirds of the chemical energy in automotive fuel is rejected to the atmosphere as waste heat. Thermomechanical stresses must be managed and TE material strength must be improved to fully exploit TE devices for waste heat recovery. Toward that, needed thermomechanical and thermophysical properties of candidate thermoelectric (TE) materials are measured in this project and then used with established probabilistic reliability and design models to optimally design automotive and heavy vehicle TE modules. Thermoelectric materials under candidacy for use in TE modules tend to be brittle, weak, and have a high coefficient of thermal expansion (CTE); therefore, they can be quite susceptible to mechanical failure when subjected to operational thermal gradients. A successfully designed TE module will be the result of the combination of temperature-dependent thermoelastic property and strength distribution data and the use of the method of probabilistic design developed for structural ceramics.

Technical Highlights

Thermomechanical and thermophysical testing of Marlow-supplied materials continued during FY11Q1. Hundreds of Bridgeman Bi_2Te_3 specimens were received from Marlow for both thermoelectric, thermoelectric, and mechanical testing. Both n- and p-type materials were received. Specimens were also harvested out of the processed billets, and several properties are being measured to determine if any positional dependencies exist.

A prototype PbTe thermoelectric module was tested at the ORNL HFIR beam line HB-2. Residual strain mapping along the heat and current flow directions was performed on p-type and n-type legs. Stress free, n-type and p-type materials were provided by Marlow as references. Neutron scans using pancake shape gauge volume (3mm x 3mm x 0.5mm) were carried out. Typical scan at each location is 20 minutes. A total of 10-12 scans were conducted in one leg. In the preliminary study a p-leg and n-leg in a 8x8 module were mapped. The residual strain profiles matched well with calculated distribution by computer simulation at Marlow.

Status of FY 2011 Milestones

1. Generate thermoelastic and mechanical property database as a function of temperature on candidate p- and n-type TEMats fabricated by Marlow Industries as part of CRADA. [Sep11] *On schedule.*
2. Refine in-situ thermal-gradient-strength test method for TEMats. [Sep11] *On schedule.*

3. Transport properties measurements of selected thermoelectric materials. [Sep11]
On schedule.

Communications/Visits/Travel

Marlow's Robin McCarty and Al Thompson visited ORNL (Wereszczak and Wang) on 21-22 Oct 2010 for a semiannual CRADA review.

Problems Encountered

None.

Publications/Presentations/Awards

J. R. Salvador, G. P. Meisner, J. Y. Cho, X. Shi, J. Yang, and A. A. Wereszczak, "Temperature Dependant Yield Strength of N- and P-Type Filled Skutterudite Materials," given at 2010 MRS Fall Meeting, Nov 29 - Dec 03, 2010, Boston, MA.

Hsin Wang, “International Round-robin Update on Thermoelectrics (Marlow Bismuth Telluride)”, Technical Symposium, International Energy Agency (IEA) Advanced Material for Transportation (AMT) semi-annual meeting, Oak Ridge, TN, Nov 9-10, 2010.

References

None.

Agreement 16308: MBD Thermoelectrics Theory and Structure

David J. Singh
Oak Ridge National Laboratory

Objective/Scope

We will use modern science based materials design strategies to find ways to optimize existing thermoelectric materials and to discover new families of high performance thermoelectrics for waste heat recovery applications in vehicles. The emphasis will be on the thermoelectric figure of merit at temperatures relevant to waste heat recovery and on other properties important for applications, especially anisotropy, cost and mechanical properties.

Technical Highlights

Vehicular applications of thermoelectric materials for waste heat recovery necessitate study and identification of high performance materials comprised of elements low in cost and abundant. This quarter we continued our recent studies of chalcogenide thermoelectrics for use in automotive waste heat recovery applications. Specifically, we conducted first principles calculations for SnS, which is a material known to have a very low lattice thermal conductivity [1] and is composed of inexpensive elements. Our calculations indicate that this material has heavy, high density of states bands and correspondingly high thermopower at substantial dopings (Fig. 1), thereby suggesting its possible use as a thermoelectric. However, we did also find substantial conductivity anisotropy. This works against high performance. However, there is potential if heavy p-type doping can be achieved. The performance of this material will ultimately depend on the (presently unknown) hole mobility at the heavy dopings where thermopowers consistent with high performance are likely.

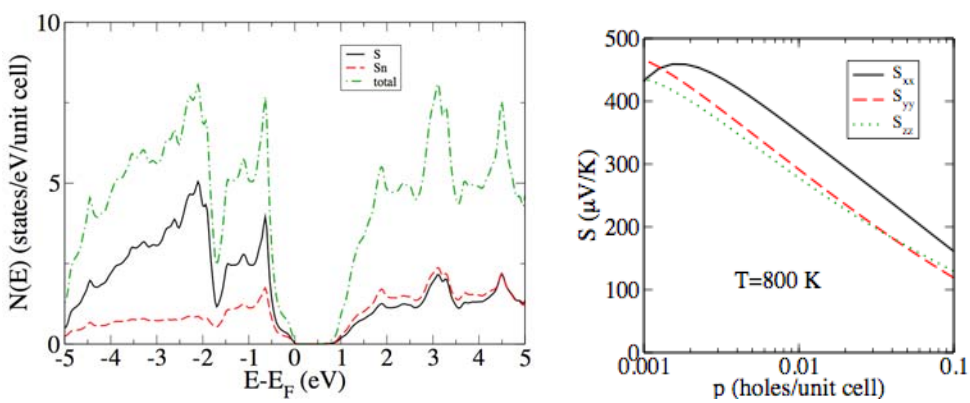

Fig. 1: Calculated density of states (left), including projection onto Sn and S orbitals, and thermopower (right) for SnS. Note the rapid rise in the density of states just below E_F and the large thermopower at dopings of 0.01 holes/unit cell.

Our Fiscal Year 2010 report detailed calculations of the lead chalcogenide thermoelectric PbSe, which has undergone surprisingly little study as a thermoelectric despite a similar chemical structure to the better known high performance material PbTe. Our theoretical analysis, presented at the 2010 International Conference on Thermoelectrics and published recently [3], suggested that if properly doped p-type this material could exhibit high temperature performance surpassing that of PbTe. We further communicated these results to an experimental group at the California Institute of Technology in order to validate this finding. This group reported preliminary results that do support our finding, and in particular the fact that PbSe has similar performance to PbTe at temperatures relevant to waste heat recovery. The importance of this is that the p-type legs in a PbTe based waste heat recovery system could be replaced with PbSe, eliminating half the Te in the system and therefore lowering cost while retaining high performance.

Also, motivated by a request from Ford Motor Company, we studied some candidate materials that could be used in "zonal" cooling applications. This requires low-cost materials with excellent performance at room temperature. We chose the copper sulfide semiconductors as both elements are inexpensive and abundant, and these materials have very low lattice thermal conductivity [1]. We analyzed the material $CuBiS_2$. Calculations revealed heavy bands near the band edges and correspondingly high thermopower (Fig. 2, left) for p-type doping, the usual doping type for this material. In addition, the conductivity (Fig. 2, right) is relatively isotropic, so that the use of polycrystalline material for production would not degrade cooling performance.

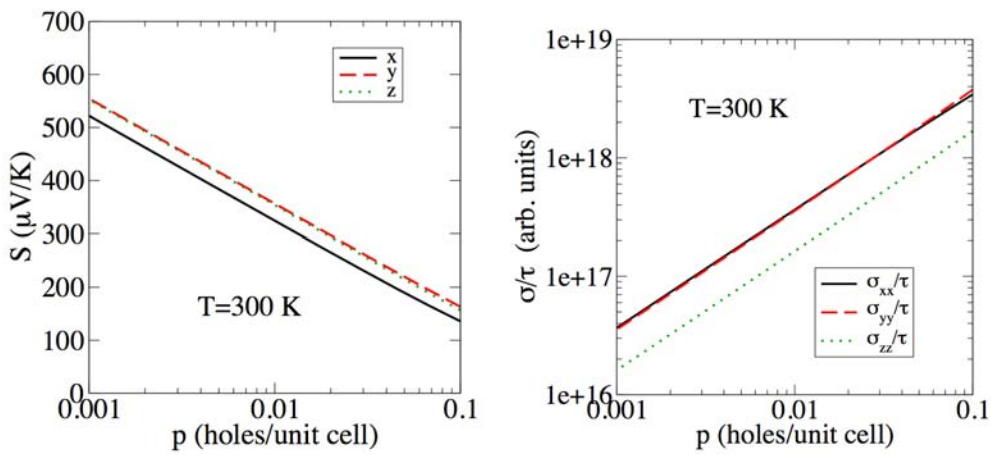

Fig. 2: Calculated p-type thermopower (left) and conductivity (right) at 300 K for $CuBiS_2$. Note the thermopowers exceeding 300 μV/K for dopings of 0.01 holes/unit cell (about 3 x 10^{19}/cm^3), and that the conductivity anisotropy does not exceed a factor of two at any doping.

Status of FY 2011 Milestones

We are making progress towards our milestone of successfully predicting new thermoelectric compositions. Future studies will include investigations of the molybdenum antimonides, as with the copper sulfides composed of inexpensive and non-toxic materials. These studies will aim to provide theoretical guidance for optimization of carrier concentration in these materials and on the effects of transition metal substitutions on this performance. Depending on the results we may continue with these efforts and/our studies of the copper chalcogenides. We also plan to study the low-cost Zintl phases as these present a wide variety of possible compositions. Finally, we are progressing on a new theoretical method for determining the electronic thermal conductivity from a set of experimental data. This is of use in cases where deviations from the Wiedemann-Franz law exist and would aid in analysis of experimental data from doped semiconductors.

Problems Encountered

No significant problems encountered this quarter.

Publications/Presentations/Awards

Refereed Papers

D. Parker and D.J. Singh, “First principles investigations of the thermoelectric behavior of tin sulfide”, Journal of Applied Physics **108**, 083712 (2010).

References

1. D.P. Spitzer, “Lattice Thermal Conductivity of Semiconductors: A Chemical Bond Approach”, Journal of Physics and Chemistry of Solids **31**, 19 (1970).

2. G.K.H Madsen and D.J. Singh, “BoltzTraP: a code for calculating band-structure dependent quantities”, Computer Physics Commun. **175**, 67 (2006).

3. D. Parker and D. J. Singh, “High-temperature thermoelectric performance of heavily doped PbSe”, Physical Review B **82**, 035204 (2010).